Universidad de Valladolid

Escuela de Doctorado Universidad de Valladolid

PROGRAMA DE DOCTORADO EN QUÍMICA: QUÍMICA DE SÍNTESIS, CATÁLISIS Y MATERIALES AVANZADOS

TESIS DOCTORAL:

COMBINING MODERN TOOLS IN THE STUDY OF PHYSICAL PROPERTIES, REACTION PROCESSES AND MECHANISMS

Presentada por Marconi Nicolás Peñas de Frutos para optar al grado de
Doctor por la Universidad de Valladolid

Dirigida por:
Prof. Dr. Pablo Espinet Rubio
Dra. Camino Bartolomé Albistegui

La Tesis Doctoral titulada *"**Combining modern tools in the study of physical properties, reaction processes and mechanism**"* ha sido realizada gracias al apoyo económico del Ministerio de Educación, Cultura y Deporte (contrato predoctoral de Formación de Profesorado Universitario, FPU-2015), al Ministerio de Economía y Competitividad (proyectos CTQ2013-48406-P, CTQ2014-52796-P, CTQ2016-80913-P, CTQ2017-89217-P), y de la Junta de Castilla y León (proyectos VA256U13, GR169, VA051P17, VA062G18, VA038G18 y UIC176).

Quiero agradecer especialmente al resto de los coautores de las publicaciones incluidas en este trabajo, Dr. Max García-Melchor, Dra. Andrea Vélez, Dra. Verónica Conejo, Dra. Zoraida Ramiro y Dra. Estefanía Gioria, así como el trabajo desarrollado por Sara Fernández en parte de los resultados presentados y que actualmente se están organizando para su publicación. Sin todas las personas que he mencionado gran parte de la tesis no podría haberse llevado a cabo. Asimismo, se agradece la ayuda puntual del Dr. José Miguel Martín, de Sergio Ferrero y de Jonathan Martínez.

Agradecimientos

El camino ha sido largo y duro, pero lo hubiese sido mucho más sin la ayuda y compañía de mucha gente especial. Sirva este espacio para agradecer a las personas que han hecho posible llegar hasta aquí.

En primer lugar, debo agradecer la dedicación incansable de los directores de tesis. Al Prof. Pablo Espinet por todo lo que he aprendido de él tanto de química como de la vida, pero más aún por haberme comprendido, y haberme apoyado siempre que lo he necesitado personal y profesionalmente. A la Dra. Camino Bartolomé por haberme captado para esta aventura, por su disponibilidad y haber tenido fe en mi desde el principio. Sin ellos no sería la persona que soy hoy.

Al Prof. Max García-Melchor por el tiempo que pasé de estancia en su grupo en el Trinity College Dublin. Por su hospitalidad y su paciencia para enseñarme a pesar de mi torpeza. También por su inestimable colaboración en parte de este trabajo. Gracias también a Eric, a Tom y Helen por hacer de la estancia una experiencia inolvidable.

A todos los profesores, especialmente a JM, por ser a la persona a la que siempre he llamado para pedir ayuda. También a Ángel y Jesús Ángel por muchos ratos juntos.

A todos los amigos de verdad que he hecho en esta etapa. A Pollo, Tomaz, Bea, Sara, Wonka y Andrea. Gracias a los cafés en compañía, ir a trabajar no ha sido tan duro y sé que cuento con ellos para lo que necesite. Al grupo de amigos de la universidad y a mis amigos de siempre, Enrique, Miguel, Adri, Chechu, Javi y María Valladares.

A los demás compañeros del QUIFIMA durante todos estos años, gracias a Vero, Estefanía, Sheila, Nacho, Estela, Desi, Marta, las dos Marías, Vanesa, Olmo, Ana, Jorge, Zoraida, Beto, Lucía, Sergio, Jaime y Rodri.

Gracias a María que ha sido la que me ha aguantado todo este tiempo y no creo que haya sido fácil. Por su paciencia y por estar siempre ahí. Eres la mejor compañera que podría tener.

A mi familia, especialmente a mis padres por su apoyo incondicional, a mi hermana y a mis abuelos. Sé que la persona a la que más ilusión le haría tener un nieto doctor me verá desde donde esté. A mi nueva familia, a Charo y a los niños.

Gracias a todos

Contents

Resumen

La investigación innovadora en química requiere cada vez más el uso adecuado y complementario de metodologías mixtas tanto experimentales como computacionales. Esta probablemente es la mejor línea argumental para relacionar los distintos proyectos abordados durante mi tesis doctoral. La memoria está dividida en cinco capítulos con temáticas muy distintas. Sin embargo, todos los trabajos comparten el enfoque conceptual y el interés de aplicar diferentes herramientas para entender profunda y rigurosamente los problemas químicos propuestos. Para ello es fundamental ser consciente del potencial, pero también de las limitaciones de cada una de las técnicas empleadas.

Las técnicas en las que más he empleado a lo largo de esta tesis han sido la resonancia magnética nuclear (RMN), las simulaciones cinéticas con software específico (COPASI), los cálculos computacionales DFT y la difracción de Rayos X. El objetivo es describir distintas estrategias de uso sinérgico de todas ellas, sin perder de vista que las herramientas computacionales son un apoyo muy valioso de los datos experimentales, pero no deben sustituirlos.

Capítulo I: ***Estudios de transmetalación Ar/Ar' y Ar/Cl en el sistema bimetálico Rh^{I}/Au^{I}***

Antes del inicio de este proyecto de tesis no existían estudios mecanísticos sobre reacciones de transmetalación entre complejos de rodio (I) y oro (I), interesantes para su eventual uso posterior en procesos de catálisis bimetálica.

Se han estudiado mecanísticamente, combinando datos experimentales, simulaciones cinéticas y cálculos DFT, dos reacciones de intercambio entre complejos de dichos metales: intercambio Ar/Ar' (Ar = haloarilo) e intercambio Ar/Cl.

Lo más llamativo de este estudio es el desigual efecto cinético observado tras la adición de cantidades variables de ligando libre ($AsPh_3$) en la velocidad de la transmetalación. Mientras que en el intercambio Ar/Ar' se ve frenado por el ligando, con un orden fraccionario y negativo, la $AsPh_3$ acelera de forma no lineal el intercambio Ar/Cl.

El perfil de reacción Ar/Ar' tiene varias etapas con estados de transición próximos en energía, produciéndose en uno de ellos la disociación de un ligando $AsPh_3$. En el caso de la transmetalación Ar/Cl hay dos mecanismos competitivos: el primero no requiere ligando adicional, y el segundo está catalizado por $AsPh_3$.

Los cálculos teóricos revelan que estas reacciones no se producen a través del mecanismo típico, si no que tienen lugar a través de procesos de inserción oxidante que conducen a intermedios con enlaces metal–metal.

<u>Capítulo II:</u> Mecanismo de intercambio de arilos en complejos de 16e con RhCp*. Efecto tampón electrónico del Cp*

Es bien conocido que la reactividad de los complejos de 18 electrones basados en el framento $Rh^{III}Cp^*$ (Cp* = pentametilciclopentadienilo) se inicia con la disociación de un ligando formando así intermedios activos de 16 electrones. Bajo esta premisa se pretendía obtener complejos pentacoordinados estables y estudiar reacciones de transmetalación.

La reacción de transmetalación con haloarilderivados de plata conduce a los complejos de fórmula $[RhCp^*Ar_2]$. El seguimiento por RMN de una disolución de $[RhCp^*Ar_2]$ y $[RhCp^*Ar'_2]$ confirma que se produce el intercambio Ar/Ar'.

La propuesta mecanística de intercambio directo a través de un estado de transición con doble puente arilo, aceptada habitualmente para otras reacciones de transmetalación, fue descartada mediante cálculos DFT. En nuestro caso, se ha podido constatar experimental y computacionalmente que el producto de hidrólisis $(\mu\text{-}OH)_2[RhCp^*Ar]_2$, presente en forma de trazas, actúa como catalizador de la reacción de intercambio.

Posteriormente se decidió investigar la elevada estabilidad de los compuestos pentacoordinados $[RhCp^*Ar_2]$, precursores de gran variedad de diaril y monoaril derivados de 18e. El análisis estructural de todos los complejos sintetizados permitió apoyar nuestra hipótesis de que el grupo Cp* responde a las variaciones de las necesidades electrónicas del centro metálico como consecuencia de la naturaleza de los ligandos que ocupan el resto de posiciones de coordinación. Hemos denominado este fenómeno como *efecto tampón electrónico del Cp**. El análisis pormenorizado de los datos estructurales nos ha permitido establecer una serie de influencia *trans* en un sistema octaédrico.

Por último, se han estudiado los correspondientes complejos con ligandos carbonilo y cianuro (CO y CN^-) mediante cálculos NBO. Este análisis demuestra la existencia de donaciones laterales de orbitales del grupo Cp* a los orbitales vacíos de estos ligandos π-aceptores. Dichas donaciones se suman a la retrodonación clásica por parte del metal y deben ser consideradas tanto en este como en otros sistemas análogos.

La primera parte demuestra la conveniencia de apoyar propuestas mecanísticas aparentemente obvias con experimentos y cálculos. La segunda es un buen ejemplo de las propuestas conceptuales que se pueden derivar de un análisis estructural profundo, por lo que este es un claro ejemplo de la importancia de un estudio exhaustivo de los datos obtenidos por difracción de rayos X.

<u>Capítulo III:</u> Reactividad de los complejos con $PdCl_2$ y ligandos PEWO coordinados como quelato

El grupo de investigación en el que he desarrollado mi tesis doctoral había diseñado previamente ligandos híbridos fosfina olefina electrónicamente deficiente (PEWO) que han dado buen resultado en catálisis de tipo Negishi y como inductores de homoacoplamientos difíciles de haloarilos con paladio. Estos ligandos poseen un esqueleto de tipo chalcona fluorada (estiril-fenil-cetona) en la olefina.

El objetivo ha sido sintetizar nuevos ligandos y estudiar su reactividad una vez coordinados a $PdCl_2$. Mientras que las PEWO libres o coordinadas únicamente por el fósforo muestran configuración *E* en la olefina, una vez coordinadas como quelato, se observa la configuración *Z* como la más estable. Dicha isomerización es posible (rápida a temperatura ambiente) gracias a la deslocalización electrónica que facilita la rotación, proceso descrito para otras olefinas de tipo chalcona. La isomerización *E/Z* requiere la disociación de la olefina del paladio, permitiendo atrapar la poco habitual configuración *Z* del doble enlace.

La configuración *Z* en la olefina es la responsable de la interesante reactividad observada en este sistema y que se inicia por un proceso de activación de un enlace C–F, geométricamente inaccesible desde la configuración *E* y, por tanto, observado únicamente tras la coordinación a paladio de forma quelato. La activación C–F y ciclación posterior conduce a la formación de complejos con ligandos híbridos fosfina-carbeno, que posteriormente experimentan procesos controlados de hidrólisis, amonólisis y oxidación con peróxidos presentes en THF *envejecido,* obteniéndose derivados con ligandos pincer PCO, PCN y bidentado PO respectivamente.

Todos estos procesos deben ser tenidos en cuenta cuando se exploren nuevas reacciones con los ligandos tipo PEWO, ya que, si son lentos, pueden interferir con la catálisis.

<u>Capítulo IV:</u> Protección de los catalizadores de Au^I frente a la descomposición mediante la adición subestequiométrica de $AsPh_3$

Los catalizadores de oro (I), generalmente denotados como $[AuL]^+$ (L = ligando neutro), formados tras la extracción de haluro con una sal de plata son extremadamente activos, por ejemplo, en reacciones de ciclación de eninos. Sin embargo, sufren rápidamente una caída abrupta en su actividad asociada a la descomposición del catalizador, proceso cuyo mecanismo apenas ha sido explorado.

Hemos demostrado experimentalmente que en el sistema [AuCl(carbeno)] la descomposición puede inhibirse completamente mediante la adición de una cantidad subestequiométrica de $AsPh_3$ tanto en condiciones catalíticas como en ausencia de enino. Afortunadamente, la actividad catalítica se mantiene, aunque su velocidad se ve disminuida ligeramente.

La protección subestequiométrica apoya el mecanismo de desproporcionación ($3Au^I$ para dar 2 Au^0 y 1 Au^{III}) para la descomposición del catalizador y permite descartar la simple reducción como fuente del oro metálico observado. El papel del ligando libre generado por equilibrios entre las especies $[AuL(W)]^+$ (W = ligando débilmente coordinado) es clave. Así, un mejor ligando, como PPh_3, no es capaz de evitar tan eficazmente la descomposición en cantidades subestequiométricas como un peor ligando, en nuestro caso $AsPh_3$.

Otros potenciales ligandos, siempre presentes en procesos catalíticos y generalmente ignorados, como son las trazas de agua en el seno de reacción son capaces de proteger pequeñas cantidades de catalizador, lo que permite explicar la actividad residual observada tras la masiva descomposición.

<u>Capítulo V:</u> Interacciones $d^8\cdots d^{10}$ y $d^{10}\cdots d^{10}$ factor clave en las propiedades fotofísicas de materiales cristalinos

Las interacciones $d^8\cdots d^8$ condicionan el color de los cristales en los complejos catiónicos de tipo $[Rh(CNR)_4]_nY_n$ (CNR = isocianuro). Asimismo, las interacciones aurofílicas $d^{10}\cdots d^{10}$ determinan la luminiscencia observada en estado sólido en los complejos [AuAr(CNR)]. Nuestro objetivo ha sido estudiar las modificaciones que podrían surgir en estos sistemas cuando se incorpora un segundo metal.

El ligando xililisocianuro es capaz de dificultar el establecimiento de interacciones de tipo π-π stacking que favorecen la formación de interacciones Rh···Rh, lo que ha permitido obtener estructuras cristalinas del complejo $[Rh(CNXylyl)_4][Au(CN)_2]$, donde las interacciones heterometálicas $d^8\cdots d^{10}$ prevalecen por completo. Estas interacciones, energéticamente débiles y condicionadas por el empaquetamiento, son las responsables del color del cristal.

Se han sintetizado complejos homometálicos del tipo [AuAr(CNPy)] (Ar = haloarilo), que presentan luminiscencia en estado sólido y mecanocromismo. El ligando 4-piridilisocianuro (CNPy) es capaz de actuar como bidentado enlazándose selectivamente a la plata por la piridina y al oro por el extremo isocianuro, de tal forma que se han podido obtener los complejos trinucleares heterobimetálicos $[\{AuAr(CNPy)\}_2Ag]BF_4$, que muestran luminiscencia naranja en estado sólido. Los cambios en la luminiscencia en todos los casos se deben a modificaciones en las interacciones Au···Au, de forma que distancias más cortas desplazan la emisión hacia el rojo.

Los datos obtenidos mediante cálculos DFT, congelando las geometrías de fragmentos representativos de las estructuras cristalinas, nos han permitido ilustrar los orbitales participantes en las transiciones electrónicas responsables de las propiedades fotofísicas observadas.

Introduction

Cutting edge research in chemistry increasingly demands the appropriate and complementary use of mixed methodologies, both experimental and theoretical. This is probably the best line of argument to relate the different projects tackled during this doctoral thesis. They may seem thematically unrelated but appearances are deceiving, they share the conceptual approach and the interest of applying different methods to obtain a deep understanding of the proposed chemical problems.

To be able to properly use the different tools, it is necessary to know their potential perfectly, but also their limitations. The decisions about how could we obtain the desired information are crucial. It is like in carpentry, you should have a complete tool box, knowing the usefulness of each tool, and not using a hammer to remove a screw.

Probably one of the critical points is deciding which problem to study and which is the most appropriate system to do it. This design is especially important if we intend to carry out a mechanistic investigation, and in this thesis a few cases are collected.

A good part of the thesis deals with mechanistic studies. For these, nuclear magnetic resonance (NMR) has undoubtedly been the most important experimental technique, applied beyond its routine use as a characterisation method.

Many of the organometallic complexes synthesized have fluorinated groups in their structures, thus allowing for their monitoring by ^{19}F NMR. The high sensitivity and large spectral width of fluorine make the spectra obtained particularly informative.

The use during the different topics (chapters I and II) of the 3,5-dichloro-2,4,6-trifluorophenyl group, denoted as Rf, stands out. Rf is chemically very similar to the more popular pentafluorophenyl group (Pf). However, the spectra recorded from the Rf derivatives, group with an AX_2 spin system, are much more informative than those of their analogues with Pf, since the absence of magnetic inequivalence allows to see small couplings (< 3 Hz). But the most important advantage is that combining the two fluorinated aryls is very much like isotopic labelling and opens a window to observation of processes (particularly group exchanges), which would be blind to the observer if monitored on one aryl only or severely distorted if two aryls with different electronic features are used. Taking advantage of these groups, we have carried out, using variable

temperature NMR experiments, detailed studies about dynamic phenomena in solution, such as restricted rotations or ligand dissociation processes.

In addition to the possibility of precise reaction monitoring, the fluorinated groups present variations in solubility, ease of crystallization and, above all, electronic modifications with respect to their non-fluorinated analogues. In the case of phosphine-olefin ligands (Chapter III), fluorine substituents radically change the observed reactivity. Moreover, the reactions with haloaryl groups involved are usually slower than with conventional aryls and therefore facilitate kinetic studies unaffordable on too fast processes with conventional aryls.

In order to carry out transmetalation studies, either R/R' or R/X exchanges (X = halide), it is necessary to evaluate both the thermodynamic and the kinetic aspects. Besides, avoiding competitive processes that can complicate the analysis is highly advisable. A clear example is the neutral ligand scrambling that is able to generate additional species within the reaction. Figure 1 shows a representative example of what happens when two organometallic complexes with different neutral ligands are mixed.

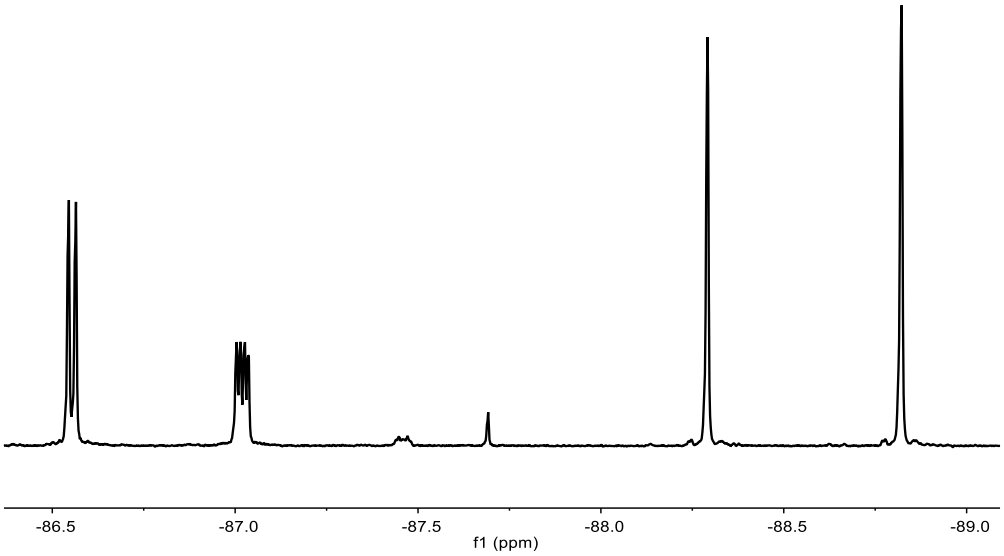

Figure 1. F^{ortho} region (^{19}F NMR spectrum) of the reaction of *trans*-[RhRf(CO)($AsPh_3$)$_2$] with *trans*-[IrRf(CO)(PPh_3)$_2$] after 30 minutes at room temperature. All *trans*-[MRf(CO)$L_xL'_{2-x}$] combinations (M = Rh, Ir) are observed.

The detailed study of a reaction mechanism is difficult enough without extra complications. Therefore, it requires a methodological planning. It is advisable avoiding mixtures with different neutral ligands, or choosing species without neutral ligands, in such a way that, if processes of this type occur, they become observationally unproductive

and undisturbing. Systems that have well preferred geometries excluding unfavorable isomerizations are occasionally of help.

The $AsPh_3$ ligand is used in several of the projects developed during this thesis. It had already yielded good results in previous works of the group. $AsPh_3$ is less oxidizable than PPh_3 and also is a far weaker ligand, making easier the processes that require ligand dissociation. However, as will be discussed in the corresponding chapters, new and unexpected effects provoked by the addition of $AsPh_3$ on the rate of different processes are reported, along with the mechanistic reasons.

Returning to the set up and procedure of kinetic studies, once the system and the measurement conditions (solvent, concentration, and temperature) have been chosen, based on a collection of preliminary experiments, we collect concentration *vs* time data of the different species detected throughout the reaction. With them, initial rates are calculated and the activation barrier for the overall process is estimated. Likewise, the kinetic orders are obtained with special interest in the influence that the addition of free ancillary ligand has on the reaction rate. Despite of our efforts, only in few occasions the detection of critical reaction intermediates is possible, because usually they are higher in energy than reagents and products.

With the experimental data acquired we carry out, when needed, non-linear adjustments by means of microkinetic modelling techniques using appropriate software (COPASI). Kinetic simulations are extremely useful and are getting more and more popular, and should become a must to verify the quality of theoretical calculations. The reason is simple, we usually considered very good results when a calculated profile does not depart more than 2 kcal mol^{-1} from the experimental data. But we cannot judge this if we do not have experimental data. An error of 2 kcal mol^{-1} translates in kinetics into an unacceptable error. For example, in chemical process carried out in normal flask conditions of temperature, a 1.5 kcal mol^{-1} difference means about 10 times rate difference. This means that experiments are very precise compared to the luckiest calculations, and must be the guide. In order to combine both methodologies and make a fine adjustment of barriers, essential in cases of competitive mechanisms or transition states (TSs) close energies, microkinetic modelling is the most suitable tool. It also makes possible to locate the energy of a TS that is difficult to calculate or with serious convergence problems, such as ligand dissociations in the gas phase.

It is clear that I am far from trying to discredit Density Functional Theory (DFT) calculations using the Gaussian package. They undoubtedly represent a particularly powerful tool, which is continually improving and will continue doing so. It is the best way to visualize and identify species that cannot be detected experimentally, such as unstable intermediates and transition states. They allow us to illustrate and support or discard mechanistic proposals. For example, in the first two chapters we discuss whether different transmetalation processes occur through typical mechanisms with the formation of a TS that displays mixed bridges or on the contrary they follow mechanisms with an "oxidative insertion" step leading to M–M bonded species. The only way to discern the mechanism in each case is calculations.

We insist, however, since this is often forgotten or neglected, that theoretical calculations must be a complement to experimental data, whenever possible, and not the other way around. In case of discrepancy it is likely that the computational model is somewhat incomplete or mistaken. There are infinite sources of error, one of them is that the active species is unknown, for example a by-product in low concentration that acts as a catalyst (an illustrative example of this case is included in the thesis). Other frequent errors are ignorance of the non-innocent nature of the solvent that can act as a ligand or issues associated with conformational complexity. And, in general steps including entropic changes, formation of ionic species, etc. so frequent in chemistry, continue being very challenging for calculation. Typically accepted "tuning" methods of calculated values are not an accepted solution when they become the norm. And this happens too often in published papers. Our best efforts are dedicated to combine the strengths of both methodologies, which in several cases I have carried in person.

Structural analysis of calculated intermediates and TSs can provide also the basis for rationalization of the reactivity studied, supporting the application of concepts such as trans influence, oxidative addition, isomerization, and others.

Another aspect in which calculations have no competitor is in the possibility they offer to carry out different orbital analyses. We have carried out in this thesis studies of both molecular orbitals (MOs) and natural bonding orbitals (NBOs) with different purposes, among which comments on metallophilic interactions or bonds (Figure 2), as well as electronic delocalizations in aromatic rings.

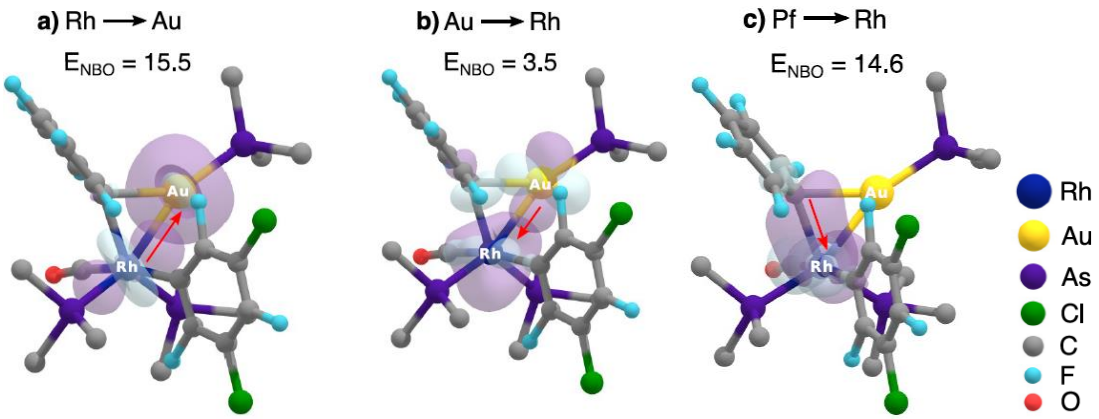

Figure 2. Selected donor-acceptor interactions in an "oxidative insertion" TS. Donation from rhodium (left) is proposed to trigger the aryl transmetalation leading to an intermediate with a Rh-Au bond (see Chapter I for details).

This type of calculations, often not needing large computational resources, have allowed us to illustrate the orbitals involved in the electronic transitions responsible for the interesting photophysical properties of crystalline materials. Regarding calculations on crystalline structures in the gas phase, it is mandatory to freeze the experimental X-ray diffraction data. If geometry optimizations using simplified models drastically alter structures, they must be avoided and restrictions must be applied. Therefore, in the case of highly simplified models that need to let out many factors such as the forces responsible for crystalline packing, the results obtained cannot aspire to be quantitatively accurate, but still they provide very interesting information.

In contrast to NMR, which provides information about the behaviour of the molecules in solution, the dynamic phenomena they experience, and their reactivity, single-crystal X-ray diffraction provides a very precise static photograph. Consequently, both are complementary. X-ray diffraction is seldom the technique for characterisation (we only examine a minute amount of the material), but sometimes it permits to clarify unexpected reactivity if the resulting products crystallize. Solving X-ray structures is easy to incorporate to the baggage of techniques and provides data in a short time, nowadays. As representative example of our use of X-ray in the thesis, in this case as collaboration in a topic of another thesis project, is the interesting structure of the by-product obtained from solutions of $[Rh(CNXylyl)_4][Au(CN)_2]$ in chloroform, hardly to identify in any other way (Figure 3).

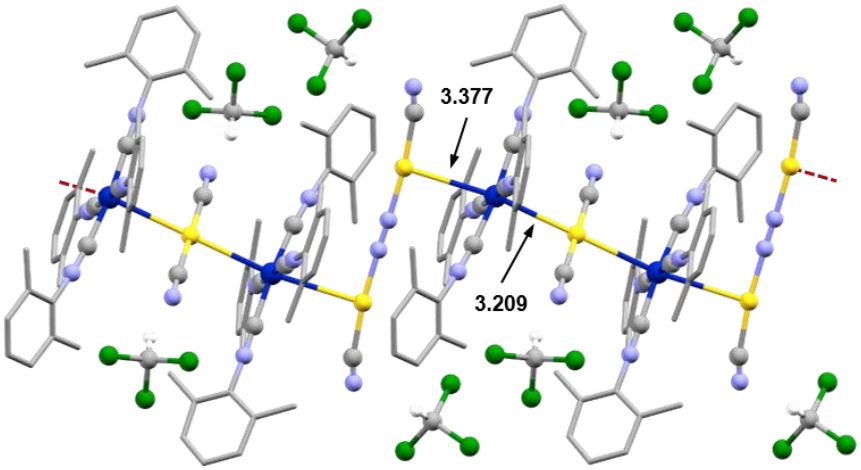

Figure 3. Ball and stick structure of the violet polymeric compound with formula $[RhL_4]_2[Au(CN)_2][Au_2(CN)_3]$. Rh···Au distances in Å. C or N in the bridging CN group of $[Au_2(CN)_3]^-$ cannot be assigned.

As I said, the crystalline structure is not necessary to characterise a species in most cases. However, our interest here was to take the structural analysis a little further, examining in detail a multitude of distances and comparing similar structures with the aim of drawing an electronic conclusion that is worth commenting on. In addition, our inspection did not end in the asymmetric unit with the analysis of a single molecule, since for that purpose, geometry optimizations using DFT can offer similar information. In the case under study, where physical properties are derived directly from the solid structure, we could help to better understand certain properties (colour, luminescence or other) by combining X-ray results and DFT calculations of appropriately selected crystal fragments.

Thus, the combination of appropriate tools is much more powerful than the simple sum of them. I am not trying to hide the fact that it is nearly impossible a perfect control of all the factors involved in the formation of a crystal, giving rise in this case to some photophysical properties. There are too many in such a delicate balance. Good examples of the complications are the dramatically different polymorphic structures obtained in several cases, even with simple molecules. However, these issues, when properly understood, enrich the conceptual discussions.

Until now I have discussed the techniques most used to obtain the results summarised in in this report. It is also worth noting the importance of observing the experiments in all aspects, even visually: a slight colour change may reveal a chemical reaction. This can be obvious, as it is the importance of reading bibliography. It may happen that the

mechanism of a new organometallic reaction is closely related to one known for related organic reactions (see chapter III).

Furthermore, the experimental ability is basic in the planning of experiments, whether synthetic or of any type. This has included work under inert atmosphere, use of low temperatures, synthesis of unreported organometallic complexes, and planning and development of catalytic and non-catalytic experiments, both in the flask and in the NMR tube. Other spectroscopic and non-spectroscopic characterisation techniques have been commonly used, such as infrared spectroscopy, especially informative in derivatives bearing carbonyl (CO) or isocyanide (CNR) ligands as well as in molecules with ketonic groups. Mass spectrometry, UV-vis and luminescence spectroscopy, including emission lifetime and quantum yield measurements, as well as powder X-ray diffraction studies have been used sporadically.

In summary, the main objective of this thesis is to describe strategies to carry out mechanistic investigations or other types of challenging studies combining the information obtained through various experimental and computational tools. It has been my privilege to have the opportunity to exploit and apply personally these several types of methodology in a synergistic way.

Chapter I: R/R' and R/Cl exchanges in the Rh^{I}/Au^{I} bimetallic system. Mechanisms and opposite kinetic effect produced by extra ligand

Bimetallic catalysis concerns homogeneous processes where two transition metals (TMs), or one TM and one Group 11 element (M), cooperate in a synthetic transformation (for example C–C coupling), in which their two catalytic cycles are linked by a transmetalation step.[1]

Our research group has much experience in the elucidation of mechanisms for different group-exchanges involving two transition metals (Au/Pd,[2] or Pd/Cu,[3] among others) by combining experimental (initial rate or kinetic orders) and theoretical (DFT calculations and kinetic simulations using the COPASI software) information.

The typical mechanistic proposal for the R^1/X (X = halide) exchange between [M]–R^1 nucleophiles and [TMR^2]–X electrophiles involves a cyclic transition-state structure with the two metals connected through mixed R^1/X bridges (equation 1). The reversibility of these processes and the eventual existence of secondary transmetalations (R^1/R^2) can complicate the result.[4]

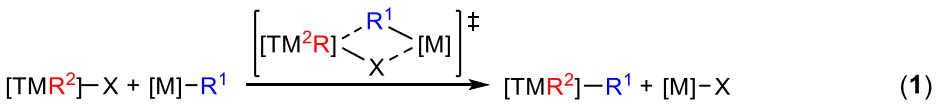

(1)

Transmetalation reactions are important not only in cross coupling processes. They can operate whenever [M]–X or [M]–R compounds (with different or identical metals) coexist in solution. Surprisingly, despite their ubiquitous presence and important

[1] (a) Pérez-Temprano, M. H.; Casares, J. A.; Espinet, P. Bimetallic Catalysis using Transition and Group 11 Metals: An Emerging Tool for C–C Coupling and Other Reactions. *Chem. – Eur. J.* **2012**, *18*, 1864. DOI: 10.1002/chem.201102888. (b) Pie, D. R.; Mankad, N. P. Bimetallic catalysis for C–C and C–X coupling reactions. *Chem. Sci.* **2017**, *8*, 1705. DOI: 10.1039/C6SC05556G.

[2] Pérez-Temprano, M. H.; Casares, J. A.; de Lera, A. R.; Álvarez, R.; Espinet, P. Strong Metallophilic Interactions in the Palladium Arylation by Gold Aryls. *Angew. Chem. Int. Ed.* **2012**, *51*, 4917. DOI: 10.1002/anie.201108043.

[3] (a) delPozo, J.; Casares, J. A.; Espinet, P. In Situ Generation of ArCu from CuF_2 Makes Coupling of Bulky Aryl Silanes Feasible and Highly Efficient. *Chem. – Eur. J.* **2016**, *22*, 4274. DOI: 10.1002/chem.201504435. (b) Pérez-Iglesias, M.; Lozano-Lavilla, O.; Casares, J. A. $[Cu(C_6Cl_2F_3)(tht)]_4$: An Extremely Efficient Catalyst for the Aryl Scrambling between Palladium Complexes. *Organometallics* **2019**, *38*, 739. DOI: 10.1021/acs.organomet.8b00885.

[4] del Pozo, J.; Salas, G.; Álvarez, R.; Casares, J. A.; Espinet, P. The Negishi Catalysis: Full Study of the Complications in the Transmetalation Step and Consequences for the Coupling Products. *Organometallics* **2016**, *35*, 3604. DOI: 10.1021/acs.organomet.6b00660.

consequences, these exchanges have been often overlooked and their mechanisms are still little studied. Recently, our group reported the drastic mechanistic switch occurring in the Ar/X exchange between SnPh(^{n}Bu)$_3$ and [Au^{I}XL] complexes: The typical concerted mechanism involving Ar/X mixed bridges operates when X = Cl, whereas an oxidative addition/reductive elimination (OA/RE) pathway *via* an Au–Sn bonded intermediate takes over when X = vinyl.[5]

As far as we know, at the start of our thesis project no studies focussed on gold(I)/rhodium(I) transmetalation reactions had been published.[6] We decided to explore the transmetalation possibilities and the mechanisms involved with this bimetallic pair. Understanding of the mechanisms of the R/X and R^1/R^2 transmetalation reactions might eventually help to the design of successful processes of bimetallic catalysis.

The two reactions studied were the Rf/Pf (Rf = $C_6F_3Cl_2$-3,5; Pf = C_6F_5) haloaryl scrambling equilibrium between *trans*-[RhRf(CO)(AsPh$_3$)$_2$] (**1**) and [AuPf(AsPh$_3$)] (**2**), and the Rf/Cl exchange between the same rhodium reactant and the chloro-gold derivative [AuCl(AsPh$_3$)] (**5**) (Scheme 1).

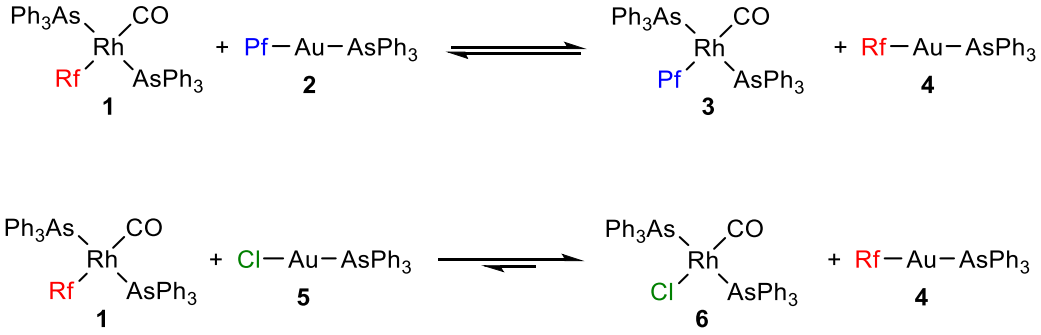

Scheme 1. Reactions studied in this work. Above: Rf/Pf exchange. Below: Rf/Cl exchange.

The Vaska type rhodium complexes used in these studies display *trans* disposition of the AsPh$_3$ ligands. These gold and rhodium complexes do not show appreciable dissociation equilibria in solution, and the use of the same ligand (AsPh$_3$) for all the complexes prevents the formation of new species *via* neutral ligand exchange, ubiquitously present

[5] Carrasco, D.; García-Melchor, M.; Casares, J. A.; Espinet, P. Dramatic mechanistic switch in Sn/Au^{I} group exchanges: transmetalation *vs.* oxidative addition. *Chem. Commun.* **2016**, *52*, 4305. DOI: 10.1039/C5CC10496C.

[6] For a Rh/Au transmetalation with Cp*Rh^{III} derivatives see: Shi, Y.; Blum, S. A. Gold and Rhodium Transmetalation: Mechanistic Insights and Dual-Metal Reactivity. *Organometallics* **2011**, *30*, 1776. DOI: 10.1021/om2001316.

in many systems in solution. Furthermore, the haloaryl groups (Rf and Pf) allow for simple and precise monitoring of the reactions by ^{19}F NMR.

The two reactions collected in Scheme 1 are selective, and neither side-products nor intermediates could be observed. However, the thermodynamics of the two processes differ, as reflected in their equilibrium constants ($K_{eq} \approx 1$ for Rf/Pf exchange; $K_{eq} \approx 7 \times 10^3$ for Rf/Cl exchange). The second and the most striking difference between both processes is the opposite effect on rate provoked upon the addition of free $AsPh_3$ (Figure 1).

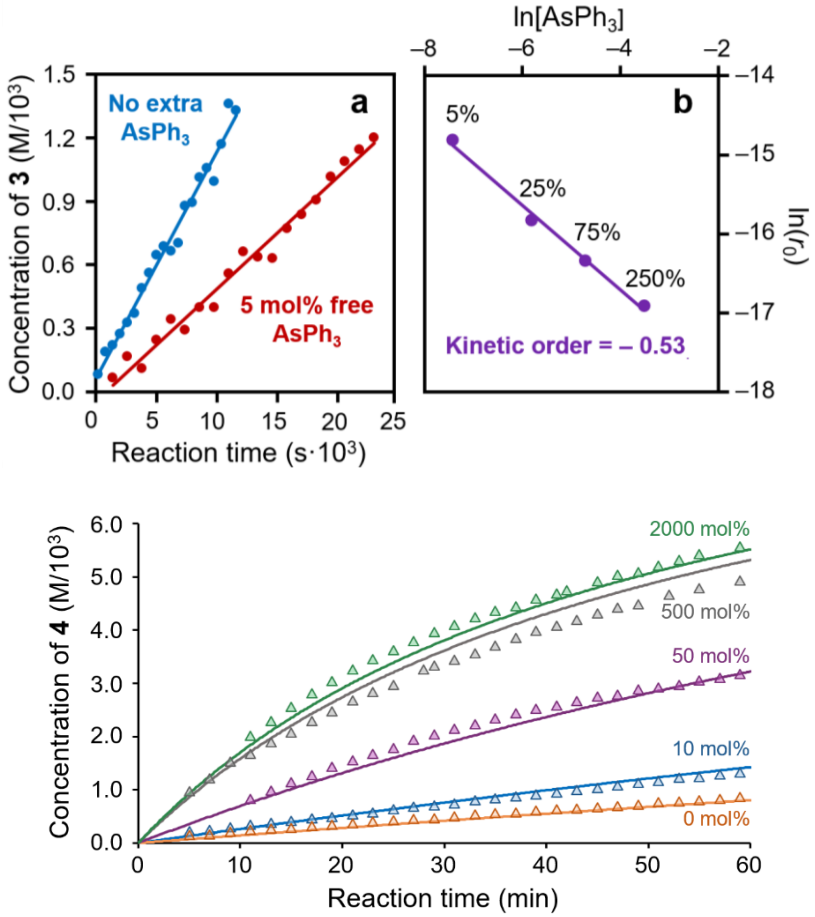

Figure 1. Kinetic effect of different amounts of added $AsPh_3$ observed by ^{19}F NMR monitoring of the corresponding reaction at a certain temperature (details in each article). Above: Data for Rf/Pf exchange. Below: Data for Rf/Cl exchange, lines represent data adjusted with COPASI overlapped with experimental data (triangles).

In the Rf/Pf scrambling, the deceleration in the presence of $AsPh_3$ deserves careful analysis. The kinetic order is fractional and close to –0.5. This deviation to the ideal order of –1 points to a Rf/Pf exchange mechanism with several steps with associated transition

states (TSs) similar in energy.[7] In one of those steps, the dissociation of one ligand must be taking place, explaining the negative order observed for the ligand. On the other hand, the fact that only 5 mol% of $AsPh_3$ added diminishes the rate to the half indicates that this 5 mol% of $AsPh_3$ relative to the starting materials must be much higher percentage relative to the species involved at the step where $AsPh_3$ dissociates.

With regard to the Rf/Cl exchange reaction, the non-linear accelerating effect of $AsPh_3$ suggests coexistence of two competitive pathways leading to the same products: one unaffected by extra ligand, and another *$AsPh_3$-catalysed*. The active species of this $AsPh_3$-catalysed mechanism must be the tricoordinate [$AuCl(AsPh_3)_2$] (**7**), indeed detected by mass spectrometry in reaction conditions. The concentrations of the two gold complexes [$AuCl(AsPh_3)$] (**5**) and [$AuCl(AsPh_3)_2$] (**7**) are connected by the ligand coordination equilibrium in Scheme 2. Kinetic simulations with COPASI software (lines in Figure 1 below) allow us to fit the equilibrium constant at 273 K (K_{eq} = 170) and the activation barriers for both pathways (19.2 and 17.7 kcal mol^{-1}, respectively).

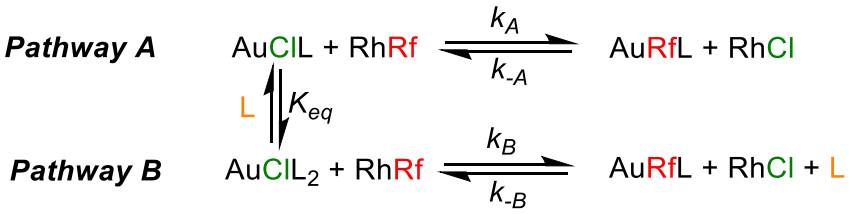

Scheme 2. Kinetic model for COPASI fitting.

With these experimental references, and taking into account that these are reversible processes, we performed DFT calculations in order to get complete mechanistic details of both exchange reactions, Rf/Pf and Rf/Cl. The mechanism proposed for the Rf/Pf exchange is a completely reversible pathway with oxidative addition and reductive elimination steps in the extremes, connected by dissociation and association $AsPh_3$ steps flanking a central rate limiting step (*rds*). This *rds* is an isomerization process between two pentacoordinated rhodium intermediates that display strong Rh–Au bonds (Figure 2).

[7] A similar fractional order was previously reported for a Pd/Au transmetalation reaction. See ref. 2.

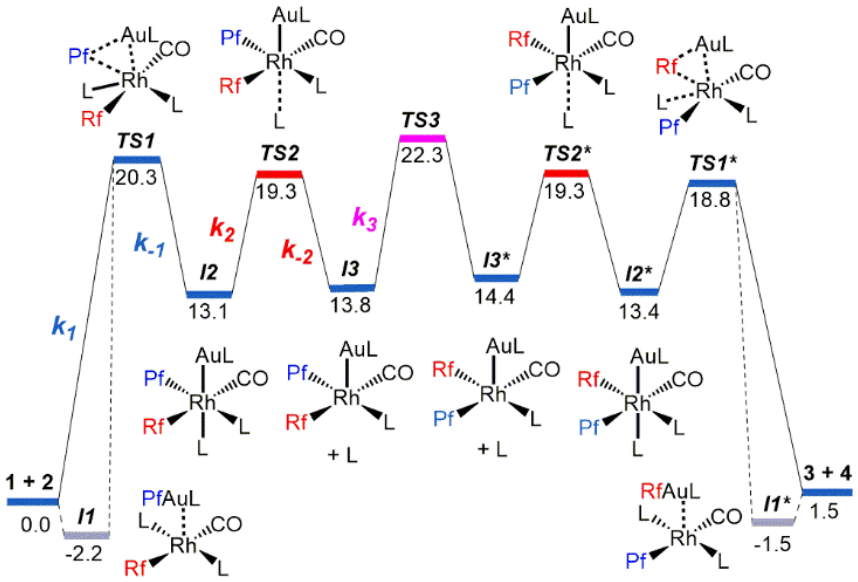

Figure 2. Gibbs energy profile combining DFT (grey and blue lines) and simulated values (red and pink lines).

The first heterometallic bonded intermediate ***I2*** is formed through a transition state (***TS1***) in which the *oxidative insertion*[8] of the rhodium centre into the Au–Ar bond occurs. Interestingly, the stereochemistry of this oxidative process differs from the one observed for the oxidative addition of H_2 to Vaska's derivative *trans*-[MCl(CO)(PPh_3)$_2$] (M = Ir, Rh) because in that case the Cl–M–CO axis undergoes angle bending.[9] In our case, the oxidative addition step is initiated by electronic donation from rhodium to gold. This favours the formation of the M–M' bond that concomitantly triggers the aryl transmetalation, as supported by NBO studies.

Regarding the Rf/Cl transmetalation reaction, since the products at both sides of the equilibrium are different, the profiles of reaction are expected to be quite asymmetric. We have calculated the two mechanistic pathways, the *uncatalysed* (Figure 3) and *ligand-catalysed* (Figure 4). Both pathways start with a TS in which the oxidative insertion of Au into the Rh–Rf bond takes place (note that in the Rf/Pf case the insertion of Rh into the Au–Pf is the one operating). The extra $AsPh_3$ coordinated to Au in **7** eases the aryl transference because it is able to weaken the Au–Cl bond that is even concomitantly cleaved in the first step of *ligand-catalysed* pathway (Figure 4).

[8] We call "oxidative insertion" to the oxidative addition giving rise to formation of a M–M' bond, since it resembles the result of that process.

[9] Vaska, L. Reversible activation of covalent molecules by transition-metal complexes. The role of the covalent molecule. *Acc. Chem. Res.* **1968**, *1*, 335. DOI: 10.1021/ar50011a003.

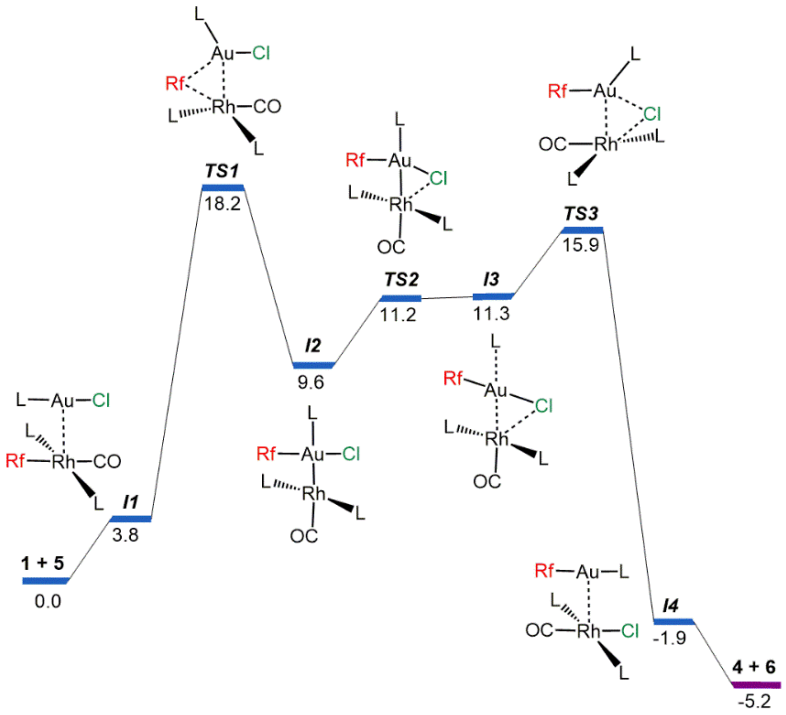

Figure 3. DFT Gibbs energy profile obtained for the uncatalysed pathway.

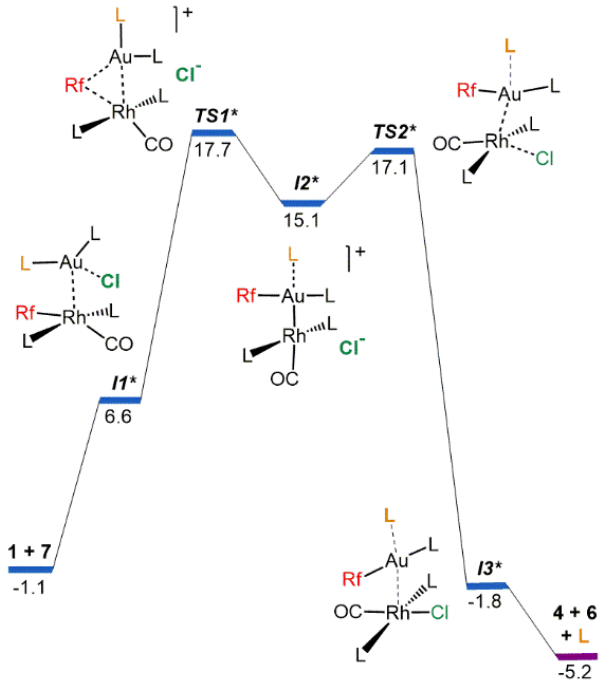

Figure 4. DFT Gibbs energy profile obtained for the $AsPh_3$-promoted pathway. Ligand labelled in orange is completely dissociated after the aryl transmetalation.

Finally, as a main and general conclusion of this Chapter, the results presented allow us to state that even very related reactions can hide completely different mechanisms and only the combination of appropriate experimental and computational techniques offers the higher chances to ascertain a mechanistic proposal. Although the possibilities offered

by both approaches have been clearly demonstrated in this study, one must also be aware of their limitations. There is also a more particular conclusion: The widely extended idea that transmetalations occur through a typical transition state with mixed bridges must be reconsidered in view of the results of this specific study. Perhaps some mechanistic proposals should be revisited, at least for oxidizable metal centres, considering an oxidative insertion alternative.

Chapter II: Unexpected Mechanism for Aryl Exchanges in 5-coordinate Rh Species Stabilized by the *Buffer effect* of Cp*. Insights into the Modulation of the Cp* Group Coordination Determined by the *Trans Influence* of the Other Ligands

Pentamethylcyclopentadienyl (Cp*) rhodium(III) and iridium(III) complexes have been widely used in organometallic chemistry since the 1960's.[10] The $M^{III}Cp^*$ 18 electron complexes typically display *piano stool* geometry, and their reactions are assumed to start with ligand dissociation to give 16e electrophilic intermediates. These 16e intermediates have been proposed as the active species in many catalytic processes, particularly in some C–H activation reactions reported very recently.[11,12]

We aimed at studying the haloaryl transmetalation possibilities in $Rh^{III}Cp^*$ derivatives using a methodology similar to that in the previous chapter. We decided to use as precursor the dimer $(\mu\text{-Cl})_2[RhCp^*Cl]_2$ (**1**), which has a modern synthesis considerably improved using microwave heating.[13] Transmetalation of **1** with the silver haloaryl derivatives AgAr·*n*NCMe (Ar = Rf, Pf)[14] afforded the deep red $[RhCp^*Rf_2]$ (**2**) and the yellow $[RhCp^*Pf_2(NCMe)]$ (**3**) complexes, respectively. Interestingly, the complex $[RhCp^*Rf_2]$ is a perfectly stable pentacoordinated species and its molecular structure differs from the typical *piano stool* geometry. The analogous $[RhCp^*Pf_2]$ (**4**), structurally equivalent to **2** (Figure 1), could be obtained heating **3** in vacuum.

[10] Kang, J. W.; Maitlis, P. M. Conversion of Dewar hexamethylbenzene to pentamethylcyclopentadienyl-rhodium(III) chloride. *J. Am. Chem Soc.* **1968**, *90*, 3259. DOI: 10.1021/ja01014a063.

[11] For a particular example of active 16e species see: Wu, Q.; Chen, Y.; Yan, M.; Lu, Y.; Sun, W.-Y.; Zhao, J. Unified synthesis of mono/bis-arylated phenols *via* Rh^{III}-catalyzed dehydrogenative coupling. *Chem. Sci.* **2017**, *8*, 169. DOI: 10.1039/C6SC03169B.

[12] For RhCp derivatives in C–H activation see: Piou, T.; Rovis, T. Electronic and Steric Tuning of a Prototypical Piano Stool Complex: Rh(III) Catalysis for C–H Functionalization. *Acc. Chem. Res.* **2018**, *51*, 170. DOI: 10.1021/acs.accounts.7b00444.

[13] Tönnemann, J.; Risse, J.; Grote, Z.; Scopelliti, R.; Severin, K. Efficient and Rapid Synthesis of Chlorido-Bridged Half-Sandwich Complexes of Ruthenium, Rhodium, and Iridium by Microwave Heating. *Eur. J. Inorg. Chem.* **2013**, *2013*, 4558. DOI: 10.1002/ejic.201300600.

[14] For other examples of silver derivatives (AgPf or $[AgPf_2]^-$) as transmetalating agents to obtain rhodium compounds see: García, M. P.; Jiménez, M. V.; Lahoz, F. J.; Oro, L. A. Synthesis and Reactivity of Mononuclear Anionic Pentafluorophenyl Compounds of Rhodium(I) and Iridium(I). X-ray Structure of $[\{P(OPh)_3\}_2(C_6F_5)_2RhAg(PPh_3)]$ *Inorg. Chem.* **1995**, *34*, 2153. DOI: 10.1021/ic00112a030.

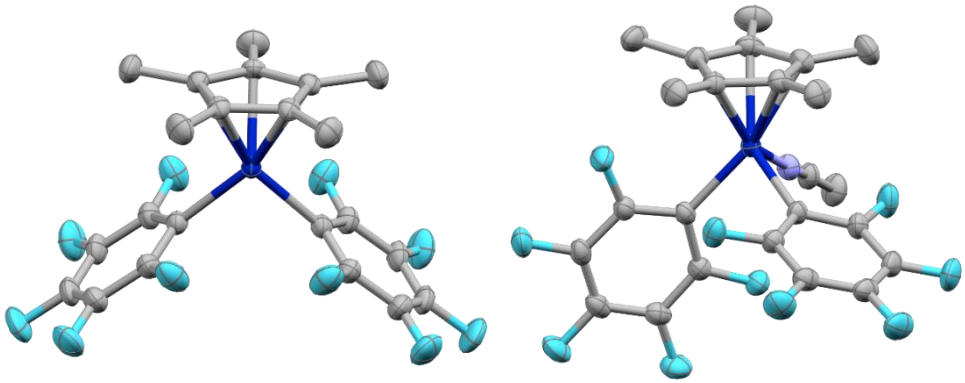

Figure 1. X-Ray structures of the 5-coordinate **4** (left) and its *piano-stool* precursor **3** (right).

These 5-coordinate derivatives **2** and **4** can be seen as models of the active intermediates formed after ligand dissociation from 18e compounds. In fact, the haloaryl scrambling reaction giving rise to the aryl-mixed species [RhCp*RfPf] (**5**) is observed at room temperature (Scheme 1). The apparently obvious mechanistic proposal for aryl transmetalation, *via* a double aryl bridged Transition State (*TS*), whether *syn* or *anti* (Scheme 1), was discarded due to the high computed activation energies that this pathway requires, close to 40 kcal mol^{-1}.

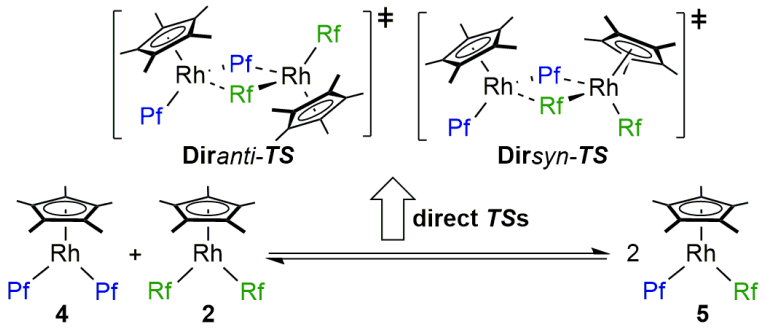

Scheme 1. Aryl scrambling equilibrium between [RhCp*Ar_2] complexes. TSs initially proposed for the direct transmetalation.

Since the direct transmetalation is not feasible, the aryl exchange observed needs the presence of a highly active species acting as catalyst. With careful experimental re-examination we managed to detect minute amounts (< 0.5 mol%) of hydrolysis products $(\mu\text{-OH})_2$[RhCp*Ar] with bridging hydroxyl groups. Luckily, we could confirm that these species are able to catalyse the aryl scrambling being studied, by acting as precursors of unobservable concentrations of 16e [RhCp*Ar(OH)] monomers. Indeed, these 16e species open the door to formation of OH-bridged TSs with accessible activation energies (Figure 2).

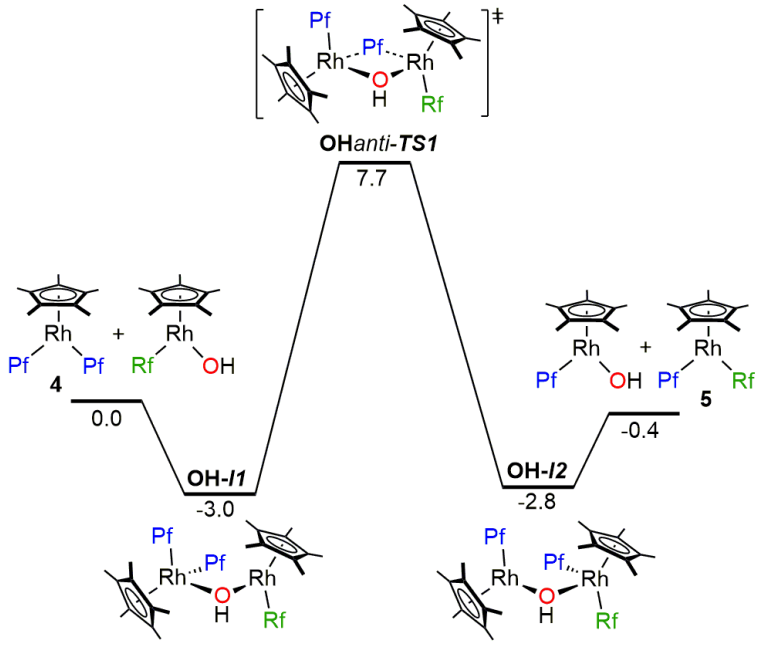

Figure 2. Gibbs energy profile for the OH-catalysed pathway with a $\Delta G^{\ddagger}$ = 10.7 kcal mol^{-1}.

The large difference of the computed activation energies for the direct and the OH-catalysed pathways can be rationalized taking a look at their associated TSs (Figure 3). While the distances in the bridging Pf group (C_6F_5) are similar, and typical for 3c2e deficient bonds, the mixed double bridge involving OH makes the difference. In the direct pathway the second aryl (Rf) is only modestly stabilizing the structure (long distance of 2.7 Å). In contrast, the OH is an extremely efficient bridging group able to form strong 2c2e Rh–O bonds, which leads to large stabilization of the corresponding TS.

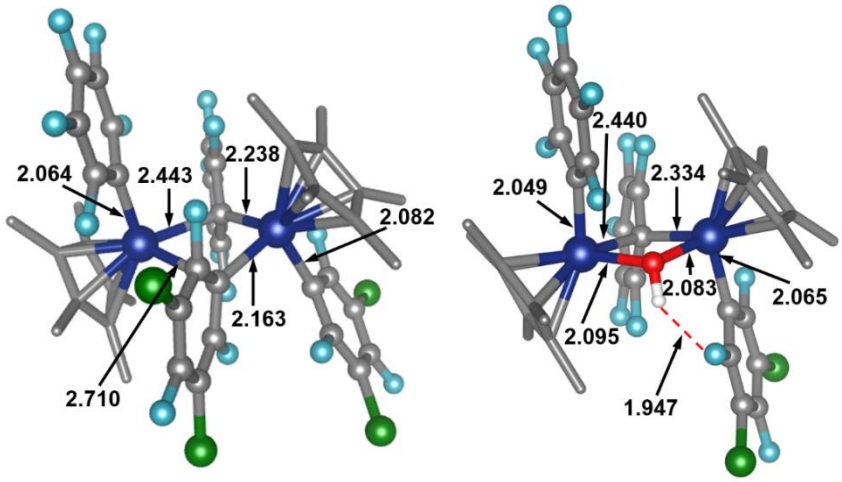

Figure 3. Calculated Transition States with relevant distances in Å.

This study is a nice example of the powerful synergistic possibilities between experiments and calculations. It must be also taken as a general warning that even apparently obvious

mechanistic proposals should, if possible, be better supported by additional data, even if they look redundant, these including computational studies.

The 5-coordinate complexes [RhCp*Ar_2] show other features that deserve further attention. Particularly, it is worth looking at the reasons for their intriguing high stability but also their potential as precursors to obtain different haloaryl compounds. Since the two fluoroaryl groups have identical reactivity, for the reactivity screening we decided to use only [RhCp*Rf_2] (**2**) because the Rf group provides simpler ^{19}F NMR spectra.

First, we approached the synthesis of octahedral 18e [RhCp*Rf_2L] compounds by ligand coordination (Scheme 2). Surprisingly, except for C-donors (CO and isocyanide), the reactions with N, P, As, S and X (X = halide) donors demonstrated to be only scarcely favourable, even with strong ligands, such as PPh_3. We could confirm that these 18e products produced ligand dissociation equilibria in solution. NMR studies at variable temperature showed that these reactions are under entropy control. In spite of this tendency to dissociation, we could obtain the molecular structures of several [RhCp*Rf_2L] derivatives, which will offer valuable information for the subsequent discussion.

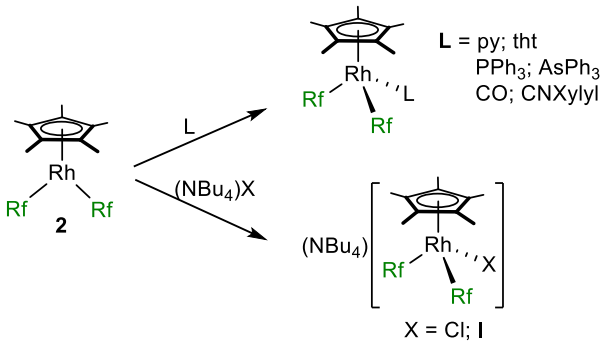

Scheme 2. Reactivity of complex **2** towards anionic and neutral ligands. Syntheses of diaryl-complexes.

Additionally, we discovered that complex **2** can be indirectly used as general precursor for monoaryl-derivatives. The selective symmetrisation reaction of **2** with **1** led to selective formation of (μ-Cl)$_2$[RhCp*Rf]$_2$ (**6**). This symmetrisation requires Rf/Cl transmetalation that, similar to the previous Ar/OH exchange, must occur *via* a TS with mixed Rf/Cl bridges. When the dimer (μ-Cl)$_2$[RhCp*Rf]$_2$ was reacted with suitable ligands, Cl-bridge splitting afforded [RhCp*RfClL] derivatives (Scheme 3).

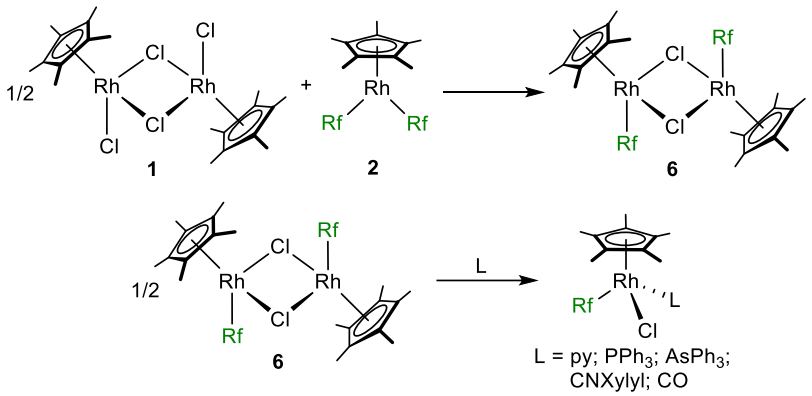

Scheme 3. Aryl-symmetrisation process to selectively form dimer **6**. Syntheses of monoaryl derivatives.

With this abundant structural information acquired we decided to go further into the structural analysis of 5- or 6-coordination of RhCp* complexes. A different case is that of the complexes with amido group, well studied in the group of Prof. Carmona (Scheme 4).[15] They have structurally characterised both pentacoordinated and hexacoordinated complexes, taking advantage of the special electronic features of the amido group, which can act as 2e ligand, but also offer extra π-donation to stabilize the pentacoordinated structure. In these complexes, the amido group compensates the ligand dissociation by bringing into play the N lone pair (Rh–N distances of 2.11 and 1.98 Å in the hexa and pentacoordinate derivatives respectively).[16] In our complexes, the Rf groups, in spite of being strong σ-donors, are not able to play the role of the amido group in the later system, and we speculated that it might be the Cp* ligand, with highly polarizable π-density, the group responsible for the electron-density compensation. Whereas this behaviour might be in as a diffuse idea in the mind of those working with MCp*, to the best of our knowledge it has never been clearly stated in spite of the enormous amount of literature published. We call it *buffer effect* of Cp*, and can be illustrated taking a look at the elongation of the Rh–Cp* distance upon coordination of ligands. For instance, the Rh–$Cp^*_{centroid}$ distances are 1.87 and 1.78 Å in [RhCp*Rf_2(CNXylyl)] and [RhCp*Rf_2], respectively.

[15] Zamorano, A.; Rendón, N.; López-Serrano, J.; Álvarez, E.; Carmona, E. Activation of Small Molecules by the Metal–Amido Bond of Rhodium(III) and Iridium(III) (η^5-C_5Me_5)M-Aminopyridinate Complexes. *Inorg. Chem.* **2018**, *57*, 150. DOI: 10.1021/acs.inorgchem.7b02283. See also references therein.

[16] Zamorano, A.; Rendón, N.; Valpuesta, J. E. V.; Álvarez, E.; Carmona, E. Synthesis and Reactivity toward H_2 of (η^5-C_5Me_5)Rh(III) Complexes with Bulky Aminopyridinate Ligands. *Inorg. Chem.* **2015**, *54*, 6573. DOI: 10.1021/acs.inorgchem.5b00905.

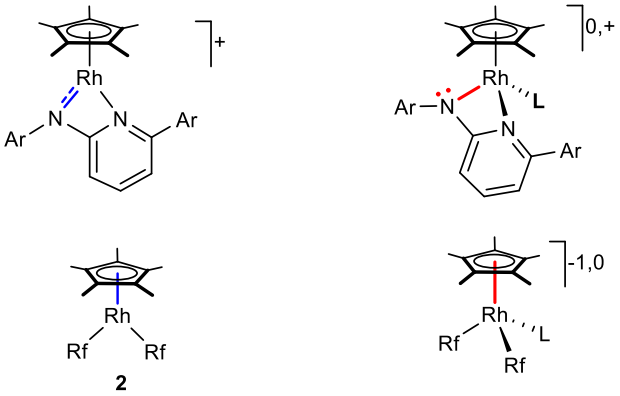

Scheme 4. Main structural differences observed upon ligand coordination to five-coordinate RhCp* species. Electronic comparison of the complexes reported by the group of Prof. Carmona (above) with our system (below).

We decided to choose the distance between the Rh atom and the centroid of the Cp* ligand as descriptor (Rh–Cp*$_{centroid}$) in order to simplify our initial structural and electronic analysis. It is well known that, in solution, the Cp* group undergoes very easy rotation, which is confirmed by the observed equivalence of the Me signals of the Cp* in ^{1}H NMR spectra recorded at low temperatures. However, but we will also analyse later the frozen structures producing inequivalence (whether from X-ray or from DFT geometry optimizations). The plot shown in Figure 4 collects the Rh–Cp*$_{centroid}$ distances obtained by X-ray diffraction studies of our complexes and others reported in the literature.

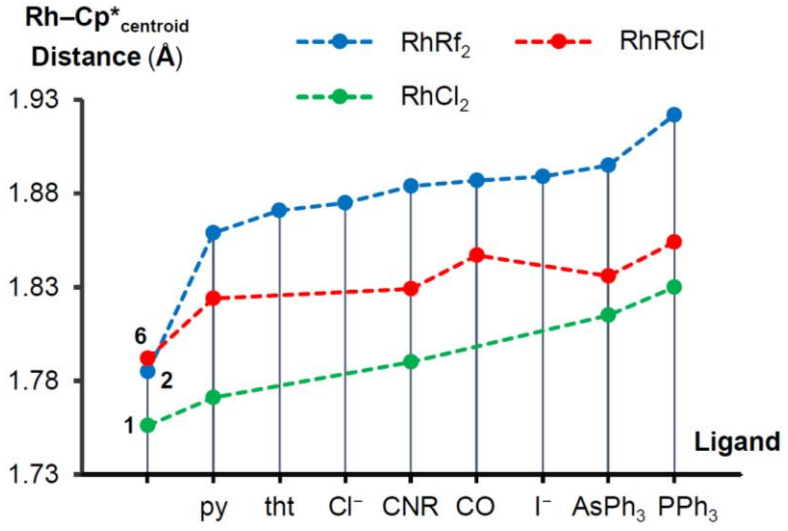

Figure 4. Plot of Rh–Cp*$_{centroid}$ distances (Å) in rhodium(III) compounds.

We classified these data in three series, for diaryl, monoaryl and dichloro derivatives (blue, red and green respectively). It is clear that the Rh–Cp*$_{centroid}$ distances are considerably shorter (meaning stronger donation from Cp* to Rh) when replacing, in

analogous complexes, strongly σ-donor Rf groups for the weaker Cl donors. This observation supports that the Cp* group compensates the variation of electron density around the metal, induced by modifications in the rest of the coordination positions. Consequently, within each series (see for example the blue one), longer Rh–$Cp^*_{centroid}$ distances must be produced by the coordination of stronger σ-donors or, what is the same, those with higher *trans influence*. This approach provided infrequent experimental observations that allowed us to rank the *trans influence* of the ligands used in an octahedral environment. The series obtained is quite similar to others reported for typical square planar complexes.[17] It should be noted that the position of the carbonyl ligand (CO) seems to be slightly different in the blue and red series (Figure 4). This is a fact often ignored and unexplained in the classical use of the *trans influence* concept, where the *trans influence* of CO is controversial, and dramatically changes its position in the series reported in different textbooks (there are also misunderstandings with the concept of *trans effect* in some papers, but this is another story).

We noted that it was probable that the position of the CO ligands might propitiate π–π* *lateral interactions* between the occupied Cp* π orbitals and the empty π* CO orbitals.[18] This conceptually alters the *trans* influence of CO as compared to the classical σ-donation and π-backdonation to and from the metal centre only. For this reason, we decided to synthesize and study related CO compounds of $M^{III}Cp^*$ (M = Rh, Ir), but also derivatives with cyanide as ligand (CN^-), isoelectronic with CO.[19] Both ligands, but specially CO, have a synergistic relationship between the backdonation received and their donor capability.[20] In fact, CO is an excellent π-acceptor (high *trans effect*) but a modest σ-donor (low *trans influence*), although its donation can be reinforced when high

[17] Hartley, F. R. The *cis*- and *trans*-effects of ligands. *Chem. Soc. Rev.* **1973**, *2*, 163. DOI: 10.1039/CS9730200163.

[18] Cp→CO donations have been established for f-metal complexes: Maron, L.; Eisenstein, O.; Andersen, R. A. The Bond between CO and Cp'_3U in $Cp'_3U(CO)$ Involves Back-bonding from the Cp'_3U Ligand-Based Orbitals of π-Symmetry, where Cp′ Represents a Substituted Cyclopentadienyl Ligand. *Organometallics* **2009**, *28*, 3629. DOI: 10.1021/om801098b.

[19] The synthesis of CN^- and CO compounds is analogous to others collected in Schemes 2-3. Ligand coordination or substitution reactions using $NBu_4(CN)$ and carbon monoxide (gas) respectively, with the corresponding precursors $[MCp^*Rf_2]$, $(\mu\text{-}Cl)_2[MCp^*Rf]_2$ or $[MCp^*Rf(NCMe)_2](SbF_6)$ afforded the desired rhodium and iridium compounds. Cationic $[MCp^*Rf(NCMe)_2](SbF_6)$ complexes were obtained by halide abstraction with $AgSbF_6$ over $(\mu\text{-}Cl)_2[MCp^*Rf]_2$ in the presence of MeCN.

[20] Ding, S.; Hall, M. B. The Rich Structural Chemistry Displayed by the Carbon Monoxide as a Ligand to Metal Complexes. *Struct. Bonding (Berlin, Ger.)* **2016**, *169*, 199. DOI: 10.1007/430_2015_208.

backdonation is available. The same applies to cyanide, although with the difference that it is a very strong donor anyway.

The backdonation being received by antibonding orbitals of the CO groups can be qualitatively measured by the ν(C≡O) wavenumbers observed in IR spectra. In our complexes, values of ν_{CO} are considerably lower in the neutral [MCp*Rf$_2$(CO)] or [MCp*RfCl(CO)] complexes than in the cationic [MCp*Rf(CO)(NCMe)]$^+$ or [RhCp*Rf(CO)$_2$]$^+$, in agreement with a less electron rich metal centre in the cationic systems. However, the widely assumed idea that the backdonation comes from the metal centre, which is often correct, needs to be modified in the Cp* complexes. As we suspected, the picture is more complex and the Cp* is not a mere spectator: it is also involved in donation to the π* orbitals of the CO group, as confirmed by NBO calculations. Figure 5 shows the comparative view of one of the typical Rh→CO back-donation NBOs, and the atypical Cp*→CO donation.

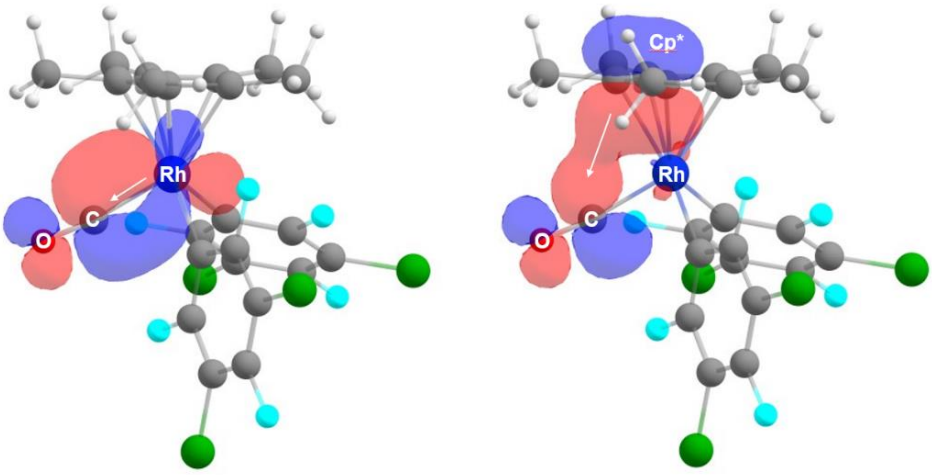

Figure 5. Pictorial view of selected NBO donor-acceptor interactions in complex [RhCp*Rf$_2$(CO)]. The orbital BD* CO is the acceptor in both cases while the donors are a LP Rh (left, E_{SOPT} = 22.8 kcal mol^{-1}) and a BD Cp* (right, E_{SOPT} = 2.5 kcal mol^{-1}). Note that there are several Rh→CO and Cp*→CO donations.

This special feature is present in different magnitude, both in CO and in CN$^-$ complexes, to lower extent in the latter because it is richer in electron density. In some cases, it reaches 10% of the total donation to the π* orbitals of CO. Moreover, the specific weight of this contribution is bigger in rhodium derivatives than in their iridium analogues. Additionally, the lateral donation is predicted to be smaller for the less donor Cp than for Cp*. This *lateral donation* is not restricted to the Cp* group but also to the other groups coordinated to the metal centre, as far as they are at appropriate distance for positive

orbital overlapping. For example, the donation coming from the Cl^- ligand in the [MCp*RfCl(CO)] complexes, is noticeably high. The analysis of several data confirmed that the typical Rh→CO backdonation represents about 80% of the total, and the other *lateral donations* can reach a not negligible 20%.

Until now, we have analysed the Cp* moiety as a group, both for the discussion of the M–Cp*$_{centroid}$ distances and for the comments on lateral donation. It is well known that its preferred coordination mode is η^5 and also that it experiments easy rotation in solution. However, examination of the frozen structures, whether from X-Ray diffraction or in DFT optimizations, confirms inevitably a clear loss of symmetry in the Cp* five-membered ring, whether in the C–C or in the Rh–C distances.

Two well understood situations of this asymmetry are represented in Figures 6[21] and 7.[22] The differences are not random and can be perfectly rationalized with the same idea of the *buffer effect* of Cp*, presented previously: the high polarizability of the π electron density of Cp* allows for compensation of the changes induced by the different donor abilities (*trans* influence) of the rest of the ligands bonded to the metal centre, and this compensation has *trans directionality*. In other words, the Cp* is tilted as can be observed attending to the clearly different Rh–C distances, and the distances to Rh are smaller for the *transoid* position(s) to the ligands with less *trans* influence. This means that a compensation of electron-density has taken place, which is reflected in the C–C distances with higher contribution of the resonance form highlighted in each case in the figures. Obviously, this tilting can be conditioned by steric hindrance issues but, in the cases selected (DFT optimized geometries without bulky groups) this steric effect is discarded. Similar tendencies are observed in the corresponding X-Ray structures. The concept of *transoid influence* should be applicable to other complexes.

[21] For ene-allyl distortion in [Rh^{I}Cp*$(CO)_2$] see: Lichtenberger, D. L.; Blevins, C. H.; Ortega, R. B. Distortions in coordinated cyclopentadienyl rings: crystal, molecular, and electronic structural analysis of (η^5-pentamethylcyclopentadienyl)dicarbonylrhodium. *Organometallics* **1984**, *3*, 1614. DOI: 10.1021/om00089a003.

[22] For diene distortion in [Pd(η^5-Cp)(PR_3)(η^1-Cp)] see: Werner, H.; Kraus, H.-J.; Schubert, U.; Ackermann, K.; Hofmann, P. Strukturdynamische organometall-komplexe: III. Synthese, struktur und bindungsverhältnisse der komplexe (η^5-C_5H_5)Pd(η^1-C_5H_5)PR_3. *J. Organomet. Chem.* **1983**, *250*, 517. DOI: 10.1016/0022-328X(83)85075-X

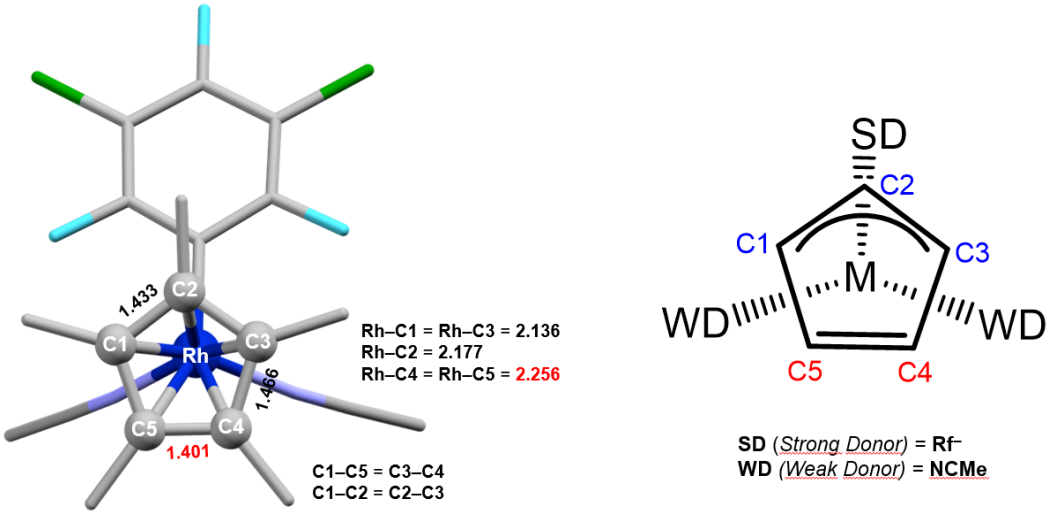

Figure 6. Zenith view of the DFT optimized structure of the cation $[RhCp^*Rf(NCMe)_2]^+$ with Cp* C–C and Rh–C distances in Å.

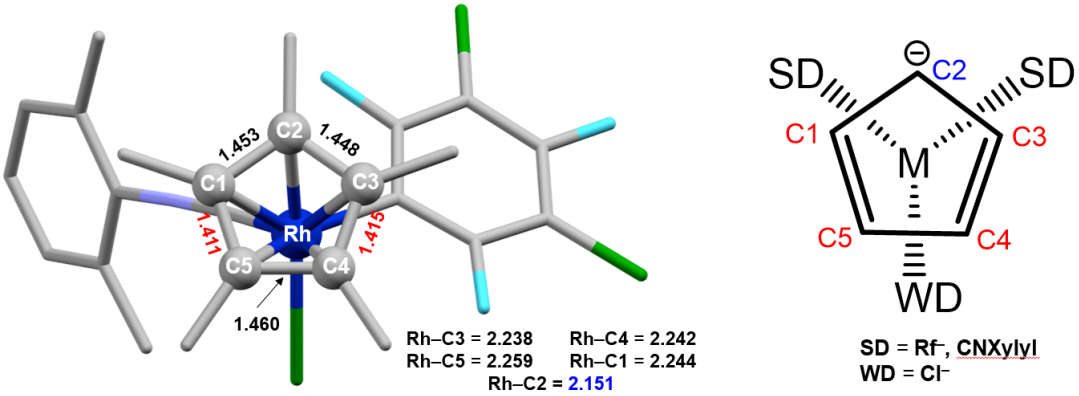

Figure 7. Zenith view of the DFT optimized structure of the complex [RhCp*RfCl(NCXylyl)] with Cp* C–C and Rh–C distances in Å.

Finally, the *indenyl effect*[23] is well known to allow for associative mechanisms through metal slippage (η^5 to η^3), thus avoiding high energy 20e transition states. This is equivalent to converting the indenyl metal centre in a pentacoordinated one. The remarkable capability of Cp* to minimize the electronic changes around the metal centre (*buffer effect*) facilitates ligand dissociation from 18e compounds to form the 16e five-coordinate intermediates needed to produce the active species required for reactivity in most cases (Scheme 5). As a numeric example, the dissociation of the strong isocyanide ligand in $[RhCp^*Rf_2(CNXylyl)]$ was computed to cost only 10.8 kcal mol^{-1}, while for the Cp analogue the computed value obtained is 17.5 kcal mol^{-1}. An appreciable effect that should be worth taking into account when selecting a system for catalytic processes,

[23] Calhorda, M. J.; Romão, C. C.; Veiros, L. F. The Nature of the Indenyl Effect. *Chem. – Eur. J.* **2002**, *8*, 868. DOI: 10.1002/1521-3765(20020215)8:4<868::AID-CHEM868>3.0.CO;2-I

because that difference might be determining to quench or facilitate the subsequent reactivity.

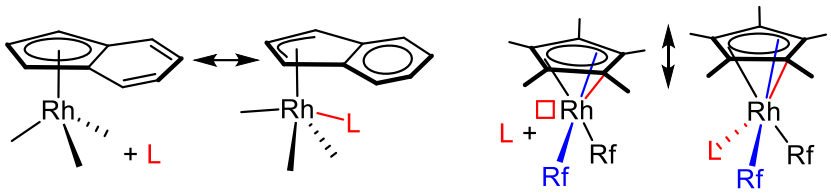

Scheme 5. Structural conversions facilitating ligand association (left: *indenyl effect*) or dissociation (right: *buffer effect of Cp**).

Two important lessons are derived from the results presented in this chapter: first, the importance to confirm even apparently obvious mechanistic proposals, because presumptions can be wrong; combination of experiments and calculations is the best way to be safe; and second, intelligent analysis of X-ray structures (or geometry optimizations) can yield much more than the routine use made of them, and help to unveil interesting electronic effects with potential consequences in the energies involved in catalyses with these complexes.

Chapter III: Reactivity of Fluorinated-Chalcone Phosphines Induced upon Coordination to $PdCl_2$. *E*/*Z* Isomerization Triggers C–F Activation

Phosphines with tethered electron withdrawing olefins (PEWO) have proven to be promising ligands for palladium catalysed cross coupling processes.[24] Particularly, our group has developed a family of PEWO where the olefin is a fluorinated chalcone (Figure 1).[25] These ligands have been successfully used in Negishi catalysis and, more interestingly, they are able to promote the challenging homocoupling of C_6F_5 from $Pd(C_6F_5)_2$ fragments as fast as the Buchwald-type ^{t}BuXPhos ligand or the extremely bulky P^tBu_3.[26]

The EWO moiety, when coordinated, diminishes dramatically the barrier for the reductive elimination step of the Pd^{II} complexes.[27] However, the Pd^0 species subsequently formed are difficult to re-oxidize.[28] For this reason, we decided to synthesize new PEWO ligands modifying either the EWO (partially fluorinated) or the PR_2 moiety (R = Cy), searching for a more convenient coupling/re-oxidation trade off.

The two new ligands PhPEWO-H_2F_2 and CyPEWO-F_4 are able to induce the Pf–Pf (Pf = C_6F_5) coupling from *cis*-[$PdPf_2(THF)_2$]. The partially fluorinated ligand behaves in an intermediate way between the more efficient PhPEWO-F_4, previously reported, and the

[24] See for example: (a) Luo, X.; Zhang, H.; Duan, H.; Liu, Q.; Zhu, L.; Zhang, T.; Lei, A. Superior Effect of a π-Acceptor Ligand (Phosphine-Electron-Deficient Olefin Ligand) in the Negishi Coupling Involving Alkylzinc Reagents. *Org. Lett*. **2007**, *9*, 4571. DOI: 10.1021/ol701995t. (b) Shi, W.; Luo, Y.; Luo, X.; Chao, L.; Zhang, H.; Wang, J.; Lei, A. Investigation of an Efficient Palladium-Catalyzed C(sp)-C(sp) Cross-Coupling Reaction Using Phosphine-Olefin Ligand: Application and Mechanistic Aspects. *J. Am. Chem. Soc*. **2008**, *130*, 14713. DOI: 10.1021/ja8049436.

[25] (a) Gioria, E.; Martínez-Ilarduya, J. M.; García-Cuadrado, D.; Miguel, J. A.; Genov, M.; Espinet, P. Phosphines with Tethered Electron-Withdrawing Olefins as Ligands for Efficient Pd-Catalyzed Aryl-Alkyl Coupling. *Organometallics* **2013**, *32*, 4255. DOI: 10.1021/om4004303. (b) Gioria, E.; Martínez-Ilarduya, J. M.; Espinet, P. Experimental Study of the Mechanism of the Palladium-Catalyzed Aryl−Alkyl Negishi Coupling Using Hybrid Phosphine−Electron-Withdrawing Olefin Ligands. *Organometallics* **2014**, *33*, 4394. DOI: 10.1021/om5005379.

[26] Gioria, E.; del Pozo, J.; Martínez-Ilarduya, J. M.; Espinet, P. Promoting Difficult Carbon-Carbon Couplings: Which Ligand Does Best? *Angew. Chem., Int. Ed*. **2016**, *55*, 13276. DOI: 10.1002/anie.201607089.

[27] Pérez-Rodríguez, M.; Braga, A. A. C.; García-Melchor, M.; Pérez-Temprano, M. H.; Casares, J. A.; Ujaque, G.; de Lera, A. R.; Álvarez, R.; Maseras, F.; Espinet, P. C–C Reductive Elimination in Palladium Complexes, and the Role of Coupling Additives. A DFT Study Supported by Experiment. *J. Am. Chem. Soc*. **2009**, *131*, 3650.

[28] Tuxworth, L. W.; Baiget, L.; Phanopoulos, A.; Metters, O. J.; Batsanov, A. S.; Fox, M. A.; Howard, J. A. K.; Dyer, P. W. Phosphine−alkene ligand-mediated alkyl−alkyl and alkyl−halide elimination processes from palladium(II). *Chem. Commun*. **2012**, *48*, 10413. DOI: 10.1039/C2CC35623F.

non-fluorinated analogue developed by Lei.[24] Moreover, the CyPEWO-F_4 is much faster but so less controlled in reactivity, suffering not only the coupling reaction but also other competitive processes.

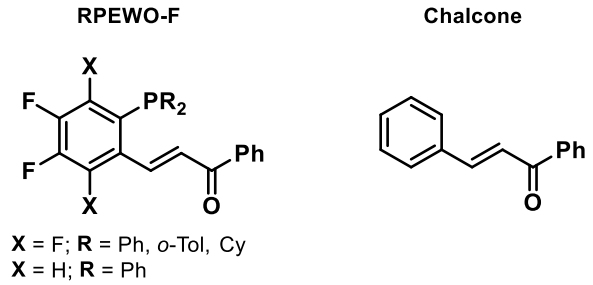

Figure 1. Fluorinated Phosphine-EWO hybrid ligands with the chalcone skeleton.

For the coupling rate measurements, a 2:1 L:Pd ratio is required to avoid ligand sequestration by the Pd^0 species. Differently, in catalytic conditions a 1:1 ratio is advisable, and the best way to achieve that is using [$PdCl_2$(PEWO-*chel*)] as precatalyst. Surprisingly, for PhPEWO-F_4 in the chelate palladium complex, the configuration of the olefin is *Z*, despite the fact that the free ligand displays *E* configuration whether in solution, solid state or coordinated as P-monodentate ligand.[25a] We tried to gain deeper insight into this olefin isomerization, and how is it feasible even at room temperature.

Scheme 1 collects the sequence of intermediates formed in the synthesis of complexes [$PdCl_2${*Z*-(RPEWO-F_4-*chel*}] (***Z*-3**) starting from *trans*-[$PdCl_2(NCMe)_2$] (**2**) and one equivalent of ligand *E*-RPEWO-F_4 (**1**; R = Ph – **a** –; *o*-tol – **b** –; Cy – **c** –). For the partially fluorinated ligand PhPEWO-H_2F_2, olefin dissociation equilibria are observed, supporting that the ligand with more fluorine groups has the stronger olefin-Pd interaction.

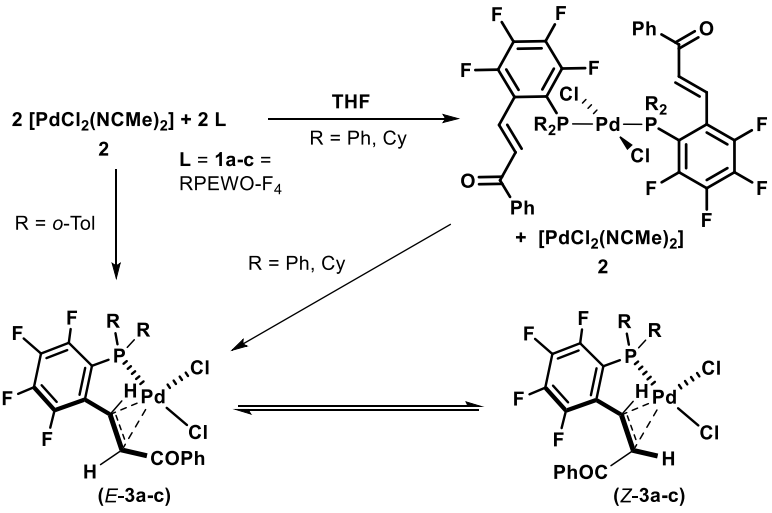

Scheme 1. Synthesis of complexes [$PdCl_2$(RPEWO-F_4-*chel*)]

Fortunately, the chelate intermediate ***E*-3b** and its *Z* isomer could be isolated and fully characterised (see Figure 2 for their X-ray structures).

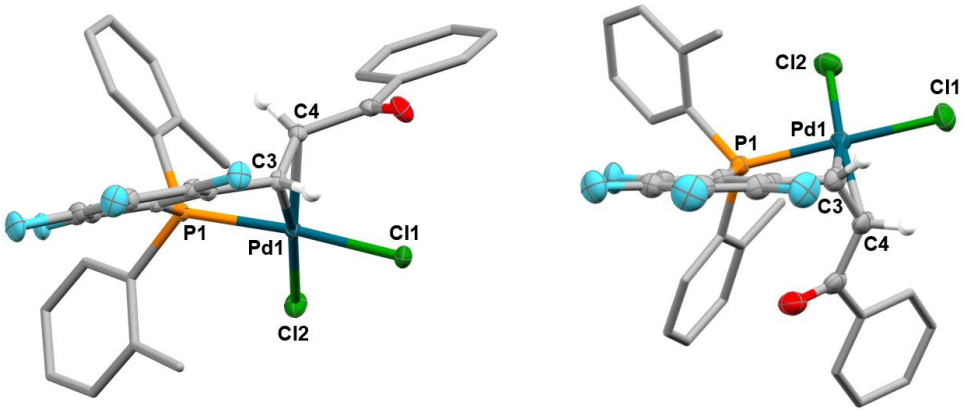

Figure 2. X-ray structures of ***E*-3b** (left) and ***Z*-3b** (right).

Either for the free PEWO ligands or the P-monodentate complexes, the *E* isomer is very thermodynamically favored. However, the chelate coordination to $PdCl_2$ reduces this thermodynamic difference and even makes the *Z*-chelate species more stable. In other words, $PdCl_2$ acts as a trap for this unusual configuration of the double bond.

The activation barrier for isomerization from the chelate complexes must be higher than from the monodentate complexes because it requires to pay first for decoordination. Complex **3b** is the only case in which the two isomers are isolable, and the availability of ***E*-3b** allowed us to carry out a kinetic study of the *E/Z* isomerization for the *o*-Tol ligand. The isomerization barriers are about 23 kcal mol^{-1} in non-coordinating solvents. Overall, these data show that the isomerization barrier is small, compared to the high activation energies for *E/Z* isomerization in common olefins. The process is catalysed by the addition of NCMe, supporting an isomerization mechanism that requires olefin dissociation to form a monodentate intermediate.

In fact, chalcone-type olefins have been reported to easily isomerize when electron-withdrawing groups are present in their skeleton due to the substantial contribution of resonance forms that reduces the activation barrier for the olefin rotation (Scheme 2).[29,30]

[29] Roque, A.; Lima, J. C.; Parola, A. J.; Pina, F. Substitution and solvent effects in the chalcones isomerization barrier of flavylium photochromic systems. *Photochem. Photobiol. Sci*. **2007**, *6*, 381. 10.1039/B612612J.

[30] In general, the barrier to rotation in regular olefins is very high, and different catalytic mechanisms have been proposed. See for example: Tan, E. H. P.; Lloyd-Jones, G. C.; Harvey, J. N.; Lennox, A. J. J.; Mills, B. M. $[(RCN)_2PdCl_2]$-Catalyzed *E/Z* Isomerization of Alkenes: A Non-Hydride Binuclear Addition−Elimination Pathway. *Angew. Chem., Int. Ed*. **2011**, *50*, 9602. DOI: 10.1002/anie.201103947.

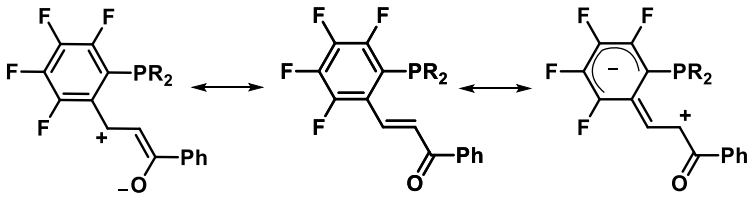

Scheme 2. Resonance forms responsible for the feasible *E/Z* isomerization and the strong electron withdrawing behaviour of these PEWO ligands when coordinated to a metal centre.

For free chalcones the *Z*-configuration can only be reached by irradiation and it is known to trigger reversible cyclization reactions with interest in optical devices.[31] Similarly, the *Z*-chelate complexes [$PdCl_2${*Z*-(RPEWO-F_4)] (***Z*-3**) with R = Ph, *o*-Tol, Cy suffer cyclization reactions with the loss of HF leading to chelate [$PdCl_2$(P-carbene)] (**4**) compounds (Figure 3). It is worth noting that their reaction rates depend strongly on the R group: they are fast at room temperature for Cy, and require higher temperatures for Ph and *o*-Tol.

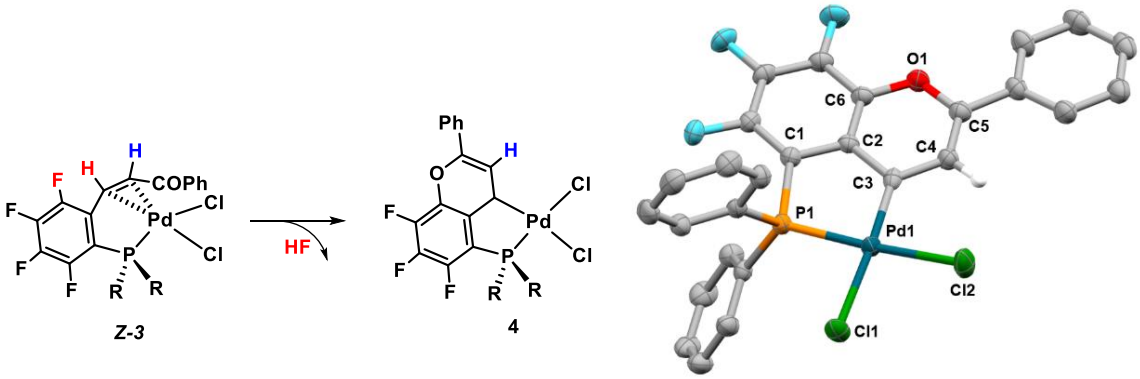

Figure 3. Cyclization reaction occurring from the *Z*-configuration of the PEWO-F_4 chelate complexes (left). X-Ray structure of the P-carbene complex [$PdCl_2$(PhP-carbene)] (**4a**) obtained.

The results of the NBO calculations have allowed us to state that an effective *aromatic* delocalization of π electron density stabilizes these P-carbene derivatives. We also predict that C3 and C5 (Figure 3) must be electrophilic. The electrophilicity of these carbon atoms is determinant for the hydrolysis and ammonolysis reactions observed subsequently. These are totally chemoselective in the nucleophilic attack to the C5 atom, forming PCO and PCN pincer complexes. On the other hand, a formal O insertion takes place in the C3–Pd bond, promoted with peroxides present in *aged* THF,[32] leading to complexes with unreported hemilabile PO ligands (Scheme 3).

[31] Pina, F.; Melo, M. J.; Maestri, M.; Ballardini, R.; Balzani, V. Photochromism of 4‘-Methoxyflavylium Perchlorate. A “Write-Lock-Read-Unlock-Erase” Molecular Switching System. *J. Am. Chem. Soc*. **1997**, *119*, 5556. DOI: 10.1021/ja9704646.

[32] For other oxidative processes promoted by these peroxides see: Zhang, B.; Cho, M.; Fortner, J. D.; Lee, J.; Huang, C.-H.; Hughes, J. B.; Kim, J.-H. Delineating Oxidative Processes of Aqueous C_{60} Preparations: Role of THF Peroxide. *Environ. Sci. Technol*. **2009**, *43*, 108. DOI: 10.1021/es8019066.

We have also made reasonable mechanistic proposals for the formation of the new complexes, which have been unambiguously characterised by X-Ray diffraction studies and other spectroscopic techniques.

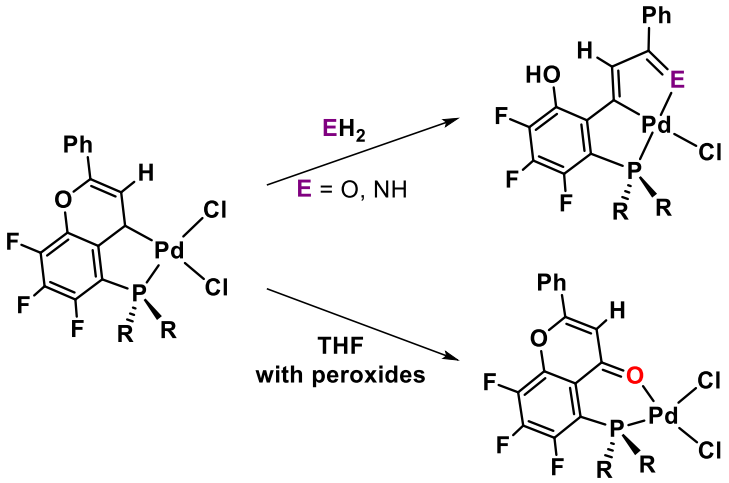

Scheme 3. Synthesis of PCE pincer and PO chelate complexes from [$PdCl_2$(RP-carbene)].

In the conclusion of this chapter, it is worth remarking that the reactivity reported is initiated by coordination of the olefin moiety to $PdCl_2$ of our chalcone-type PEWO-F_4 ligands. The coordination favours the *E*/*Z* isomerization, which triggers the C–F activation process that follows. Neither the isomerization nor the subsequent reactivity is observed without the ligand in a chelate mode.

These processes should be taken as a warning for reactions using fluorinated PEWO ligands, because the reactivity observed can interfere in the results when exploring new catalytic processes, if these are not fast enough or if harsh conditions are required. At least for the Negishi catalyses reported so far by the group,[25] using strong nucleophiles and room temperature, this has not happened.

Chapter IV: Protection of Gold(I) Catalysts by Substoichiometric Agents. Is the Decomposition to Metallic Gold a Simple Reduction?

Gold(I) has become a widely used catalytic metal. Its ability to promote cyclizations reactions over organic substrates is particularly prolific.[33] Interesting bimetallic catalytic processes involving Au^{I} have been also recently reported by our research group.[34]

The formation of gold(0) nanoparticles during catalysis using *naked* [AuL]$^{+}$ species is very frequent,[35] but is usually not mentioned because the extremely fast kinetics lead to high conversions anyway with low loads of catalyst. However, this decomposition produces an important decay of the catalytic activity and also prevents the recyclability of the catalyst. Moreover, the formation of gold nanoparticles lets open the question of whether they participate in the catalysis.

Au^{0} is apparently formed in the absence of obvious reducing agents. Interestingly, some works, not focussed in catalysis, reported disproportionation processes of 3Au^{I} into 2Au^{0} + Au^{III}, as synthetic protocol to obtain both nanoparticles[36] or gold(III) derivatives.[37] Previous to these articles, Jones *et at* were able to demonstrate that [AuXL] complexes (L = picoline) disproportionate in part into gold(III) and gold(0) when 50% of the halide is extracted with a silver salt (equation 1).[38] Curiously, these results had been unnoticed in the area of gold catalysis for many years until our work.

$$4\,[Au^{I}ClL] + 2\,Ag(SbF_6) \longrightarrow [Au^{I}L_2](SbF_6) + [Au^{III}Cl_2L_2](SbF_6) + 2\,Au^{0} \qquad (1)$$

[33] (a) Dorel, R.; Echavarren, A. M. Gold(I)-Catalyzed Activation of Alkynes for the Construction of Molecular Complexity. *Chem. Rev.* **2015**, *115*, 9028. DOI: 10.1021/cr500691k (b) *Modern Gold Catalyzed Synthesis*; Hashmi, A. S. K.; Toste, F. D.; Eds.; Wiley-VCH: Weinheim, Germany, **2012**.

[34] delPozo, J.; Carrasco, D.; Pérez-Temprano, M. H.; García-Melchor, M.; Álvarez, R.; Casares, J. A.; Espinet, E. Stille Coupling Involving Bulky Groups Feasible with Gold Cocatalyst. *Angew. Chem. Int. Ed.* **2013**, *52*, 2189. DOI: 10.1002/anie.201209262.

[35] *Naked* or monocoordinated [AuL]$^{+}$ are commonly proposed as the catalytically active species formed after halide extraction over [AuXL] complexes with a silver salt.

[36] Bergamini, G.; Ceroni, P.; Balzani, V.; Gingras, M.; Raimundo, J.-M.; Morandi, V.; Merli, P. G. Synthesis of small gold nanoparticles: Au(I) disproportionation catalyzed by a persulfurated coronene dendrimer. *Chem. Commun*. **2007**, 4167. DOI: 10.1039/B708115D.

[37] See for example: Rana, B. K.; Nandy, A.; Bertolasi, V.; Bielawski, C. W.; Saha, K. D.; Dinda, J. Novel Gold(I)− and Gold(III)−N-Heterocyclic Carbene Complexes: Synthesis and Evaluation of Their Anticancer Properties. *Organometallics* **2014**, *33*, 2544. DOI: 10.1021/om500118x.

[38] Jones, P. G.; Ahrens, B. Gold(I) Complexes with Amine Ligands, II. Methylpyridine Complexes of Gold(I). *Z. Naturforsch., B: J. Chem. Sci.* **1998**, *53*, 653. DOI: 10.1515/znb-1998-0702.

As far as we know, before the start of this thesis, only one work published by the group of Hammond faced the question of the decomposition of gold complexes under catalytic conditions. The authors proposed that unsaturated organic substrates might induce disproportionation and they also managed to detect Au^{I}, Au^{0} and Au^{III} by XPS spectra from solutions of [Au(OTf)(PPh_3)] with cyclohexene in chloroform.[39]

In this context, we decided to study the decomposition of our [AuCl(carbene)] catalysts (carbene = NAC = Nitrogen Acyclic Carbene) successfully used in cyclization of 1,6-enynes (equation 2).[40] These complexes are very active when Cl is extracted with $Ag(SbF_6)$, but formation of gold nanoparticles was clearly observed during the catalyses. The cationic $[Au(AsPh_3)(NAC)]^{+}$ was also active and also much slower. To our surprise we soon discovered that a stoichiometric amount of $AsPh_3$ was not necessary to protect the catalyst from decomposition. Indeed, just a very substoichiometric amount of $AsPh_3$ (10 mol%) was totally efficient in the protection of the catalyst,[41] quenching the decomposition while only slightly decelerating the catalysis and allowing for higher turnover numbers.

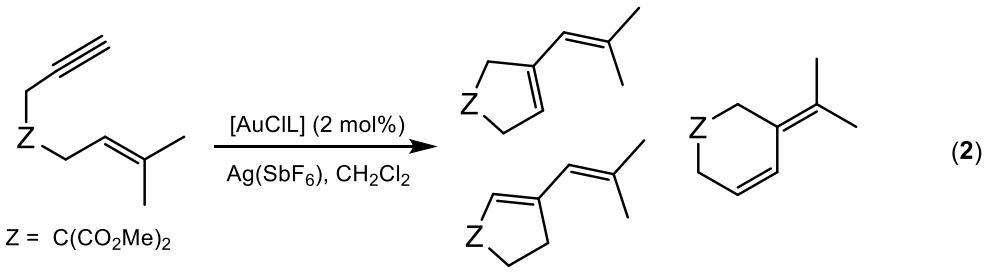

(**2**)

As a picture is worth a thousand words, the difference between two catalytic reactions (with and without substoichiometric protection with $AsPh_3$, after 30 minutes) is shown in Figure 1. Obviously we had to focus the work to understanding this unexpected case. And for this it was also necessary to elucidate whether the formation of Au^{0} nanoparticles in the catalytic processes was a disproportionation or a reduction process.

---

[39] Kumar, M.; Jasinki, J.; Hammond, G. B.; Xu, B. Alkyne/Alkene/Allene-Induced Disproportionation of Cationic Gold(I) Catalyst. *Chem. – Eur. J.* **2014**, *20*, 3113. DOI: 10.1002/chem.201304271.

[40] (a) Bartolomé, C.; Ramiro, Z.; García-Cuadrado, D.; Pérez-Galán, P.; Bour, C.; Raducan, M.; Echavarren, A. M.; Espinet, P. Nitrogen Acyclic Gold(I) Carbenes: Excellent and Easily Accessible Catalysts in Reactions of 1,6-Enynes. *Organometallics* **2010**, *29*, 951. DOI: 10.1021/om901026m. (b) Bartolomé, C.; García-Cuadrado, D.; Ramiro, Z.; Espinet, P. Exploring the Scope of Nitrogen Acyclic Carbenes (NACs) in Gold-Catalyzed Reactions. *Organometallics* **2010**, *29*, 3589. DOI: 10.1021/om100507r.

[41] Ramiro, Z.; Bartolomé, C.; Espinet, P. Protection of the Gold(I) Catalyst by $AsPh_3$ in Reactions of Enynes. *Eur. J. Inorg. Chem.* **2014**, *2014*, 5499. DOI: 10.1002/ejic.201402744.

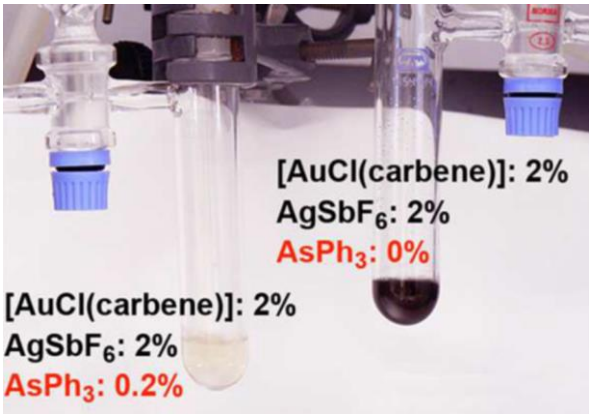

Figure 1. Aspect of the enyne cyclization experiments after 30 minutes: with added $AsPh_3$ (left) and without added $AsPh_3$ (right).

First, we confirmed that the decomposition occurs also out of a catalytic reaction too, when a chloro complex [AuCl(carbene)] reacts with the stoichiometric amount of $AgSbF_6$ in the non-coordinating CH_2Cl_2. Thus, there is at least one efficient decomposition pathway that does not need to be induced by the presence of enyne or any other reagent.

We could also demonstrate that the almost total loss of activity is not due to complete reduction of the gold(I) catalyst to metallic gold. In fact, the catalytically inactive complex $[Au(carbene)_2]SF_6$ (carbene = {C(NHXylyl)(NMe_2)}), could be isolated upon halide abstraction. The analogous complex was detected by Jones in the disproportionation reaction showed in equation 1.

After halide abstraction, the existence of monocoordinated $[AuL]^+$ species in solution is extremely unlikely. Indeed, it seems more realistic to propose the existence of multiple equilibria between species of the type $[AuL(W)]^+$, in which W represents any fairly weak ligand such as water in the solvent, the solvent itself, unsaturated products in catalytic experiments, or the Y anion, and also $AsPh_3$ or any other ligating species when available.

Under catalytic conditions, catalysis and decomposition are two competitive pathways, that must proceed from different intermediates: *i*) $[AuL(enyne)]^+$, mononuclear intermediates in the cyclization of enynes; and *ii*) polynuclear species $[Au_nL_n(W)_m]^{+n}$ ($n \geq 3$; $n > m$) formed from [AuL(W)]Y, assuming the disproportionation mechanism as the most plausible decomposition way.

A simple analysis might lead to the inaccurate conclusion that if a 10 mol% of $AsPh_3$ reacts with 100 mol% of $[AuL(W)]^+$ (formed after halide extraction) a 10 mol% of $[AuL(AsPh_3)]^+$ and no free $AsPh_3$ will be available in solution. If that were the case, no protection should be observed for the other 90 mol% of unprotected gold. Moreover, if

$AsPh_3$ were not involved in associative ligand substitution equilibria, at least with the enyne, the cationic complex $[AuL(AsPh_3)]^+$ would be totally inactive for enyne cyclization catalysis. But, as commented before, this is not the case. Scheme 1 shows the competitive mechanisms of catalysis and decomposition under substoichiometric protection, highlighting the role of arsine in both cases.

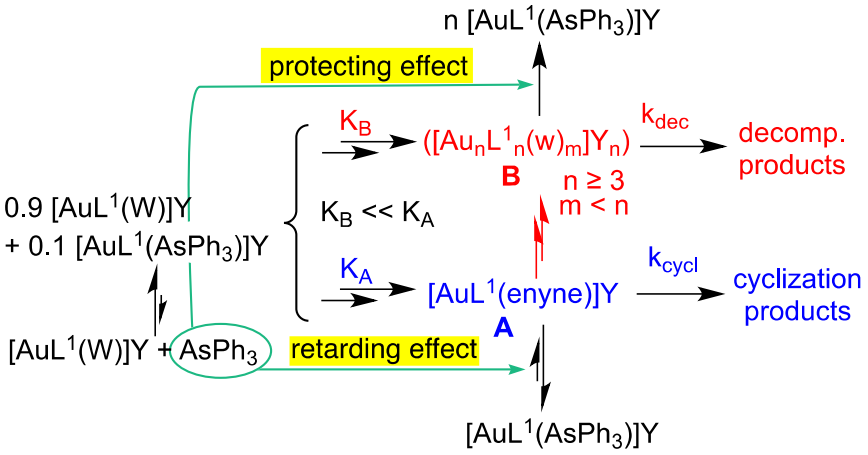

Scheme 1. Decomposition (red) *vs* Catalysis (blue).

Upon addition of a substoichiometric (10 mol%) amount of $AsPh_3$, the minute concentration of free $AsPh_3$ generated in equilibrium with different W donors must, however, be huge compared to the minuscule concentration of polynuclear aggregates, which are the proposed intermediates in the pathway to decomposition. Consequently, these are destroyed by arsine coordination, quenching the decomposition. The addition of a substoichiometric amount of $AsPh_3$ certainly diminishes the concentration of the key mononuclear intermediates involved in the catalysis, but it is deadly for the decomposition process. In other words, although it somewhat reduces the *kinetic catalytic efficiency*, in exchange it supresses the decomposition. No doubt this is an excellent trade-off.

In order to support this unconventional idea, we hypothesized that substoichiometric amounts of a strong-coordinating ligand, such as PPh_3 should lead to only negligible concentrations of free ligand, insufficient for good protection of the rest of the catalyst. Thus, the best ligand in stoichiometric protection should be the worst in substoichiometric protection. In effect, to our delight, PPh_3 protects the catalyst less efficiently than $AsPh_3$, as clearly shown in Figure 2.

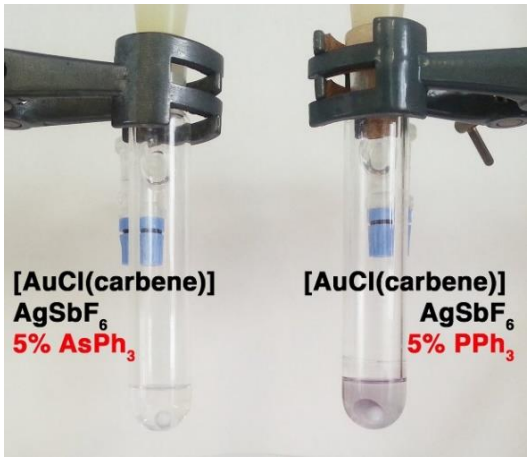

Figure 2. Aspect of reactions with the same substoichiometric amount of $AsPh_3$ (left) and PPh_3 (right) after 9 hours.

We observed that the unprotected catalyst is able to preserve some of its initial activity (less than 10% after 15 minutes in some cases). This is due to the presence of silent ligands such as adventitious water. The results of the catalytic experiments obtained upon consecutive cycles with the unprotected (except for the adventitious water) catalyst (blue) and the substoichiometrically protected (red) are shown in Figure 3. While the diminished catalytic rates remain constant for the protected system, the activity of the unprotected catalyst quickly decays. As in Aesop's Fable, *The Hare and The Tortoise*: a fast unprotected catalyst loses the race against a slower but protected catalyst.

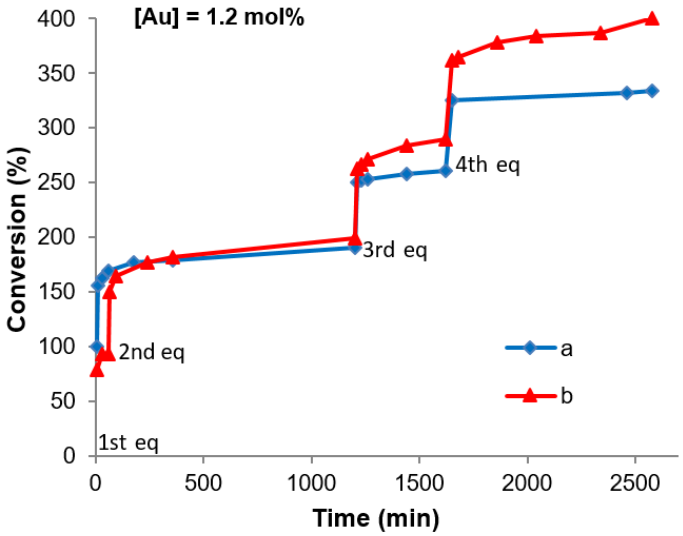

Figure 3. Successive enyne cyclization reactions with 1.2 mol% of Au catalyst. Experiment without added $AsPh_3$ (blue) and with a 10 mol% of added $AsPh_3$ with respect to the gold (red).

As the main conclusion of this chapter, the unusual effect provoked by the addition of substoichiometric amounts of $AsPh_3$ over the decomposition of gold complexes cannot be explained by a mononuclear reduction mechanism, and requires the operation of a

multinuclear disproportionation mechanism which involves the participation of, at least, three Au^I molecules. These results provide a good starting point for improving catalytic systems based on *naked* gold(I) intermediates. Similar strategies might be used to increase the turnover numbers, reduce the loads of catalyst or enable their use at higher temperatures, avoiding decomposition but maintaining a still satisfactory catalytic activity.

Chapter V: The Key Role of $d^8\cdots d^{10}$ and $d^{10}\cdots d^{10}$ Interactions in the Photophysical Properties of Crystals. Packing *vs* DFT

Self-Assembled materials based on d^8 and d^{10} transition metal complexes have been widely studied, and their properties are tightly connected to the absence, presence and strength of metallic interactions.[42] These interactions usually are far weaker than a chemical bond. Consequently, they can often be observed only in solid state, because they are lost in solution.

We have chosen two systems that have proven to display interesting photochemical properties. On the one hand, rhodium(I) cationic complexes of the type $[Rh(CNR)_4]^+$, which show colours that typically depend on the existence of $d^8\cdots d^8$ interactions. On the other, luminescent gold(I) complexes [AuAr(CNR)] (Ar = haloaryl) complexes, which display emissions that are determined by aurophilic interactions ($d^{10}\cdots d^{10}$). In this chapter we provoke modifications on these systems adding a second metal.

In the case of $[Rh(CN\mathbf{R})_4]^+$ complexes, these often display deep colours in the solid state, derived from the fact that they give rise to homometallic Rh···Rh interactions.[43] When arylisocyanides were used, those interactions are associated to the concomitant formation of strong π-stacking. Particularly, in a work reported by the group of Grimme, they estimate that in the dimer $[Rh(CNPh)_4]_2^{2+}$, the contribution to stability of the Rh···Rh interaction is less than 15% to the total binding energy and the rest corresponds to the *intra-unit* π-stacking.[44] As modification we decided to use the more sterically demanding xylylisocyanide, CN**Xylyl** in order to hamper the π-stacking. The consequence was that we obtained a yellow species $[Rh(CNXylyl)_4](BF_4)$ (**1**) with no Rh···Rh interactions in

[42] (a) Wong, K. M.-C.; Au, V. K.-M.; Yam, V. W.-W. 8.03- Noncovalent metal-metal interactions. In *Comprehensive Inorganic Chemistry II*, 2nd ed.; Reedijk, J., Poeppelmeier, K., Eds.; Elsevier: Oxford, U.K., **2013**; pp 59. DOI: 10.1016/B978-0-08-097774-4.00813-5. (b) Yam, V. W.-W.; Au, V. K.-M.; Leung, S. Y.-L. Light-emitting self-assembled materials based on d^8 and d^{10} transition metal complexes. *Chem. Rev*. **2015**, *115*, 7589. DOI: 10.1021/acs.chemrev.5b00074.

[43] See for example: (a) Tran, N. T.; Stork, J. R.; Pham, D.; Olmstead, M. M.; Fettinger, J. C.; Balch, A. L. Variation in crystallization conditions allows the isolation of trimeric as well as dimeric and monomeric forms of $[(alkyl\ isocyanide)_4Rh^I]^+$. *Chem. Commun*. **2006**, 1130. DOI: 10.1039/B513700D. (b) Chan, A. K. W.; Wong, K. M.-C.; Yam, V. W.-W. Supramolecular Assembly of Isocyanorhodium(I) Complexes: An Interplay of Rhodium(I)···Rhodium(I) Interactions, Hydrophobic-Hydrophobic Interactions, and Host-Guest Chemistry. *J. Am. Chem. Soc.* **2015**, *137*, 6920. DOI: 10.1021/jacs.5b03396.

[44] Grimme, S.; Djukic, J.-P. Cation−Cation "Attraction": When London Dispersion Attraction Wins over Coulomb Repulsion. *Inorg. Chem.* **2011**, *50*, 2619. DOI: 10.1021/ic102489k.

the solid X-ray structure. However, several π-stacking *inter-unit* interactions are observed in the crystalline packing, which are responsible for the stability of the crystal.

Having precluded the intra-unit interactions, we decided to add the dicyanoaurate anion $[Au^{I}(CN)_2]^-$. These anions are known to make Au···Au aurophilic interactions in solution.[45] Our purpose was to induce Rh···Au interactions supported by charge attraction, at the expense of π-stacking in Rh or Au···Au in gold. Whereas this does not happen in solution, it was achieved in the solid state. Anion metathesis on **1** produced the desired $[Rh(CNXylyl)_4][Au(CN)_2]$ (**2**), which is yellow in diluted solutions because the ions are dissociated (dicyanoaurate is colourless and monomeric RhL_4^+ is yellow). However, in the solid state everything changes. Fortunately, we could characterise three different polymorphs depending on the crystallisation conditions, which are orange, deep blue and green respectively (Figure 1).

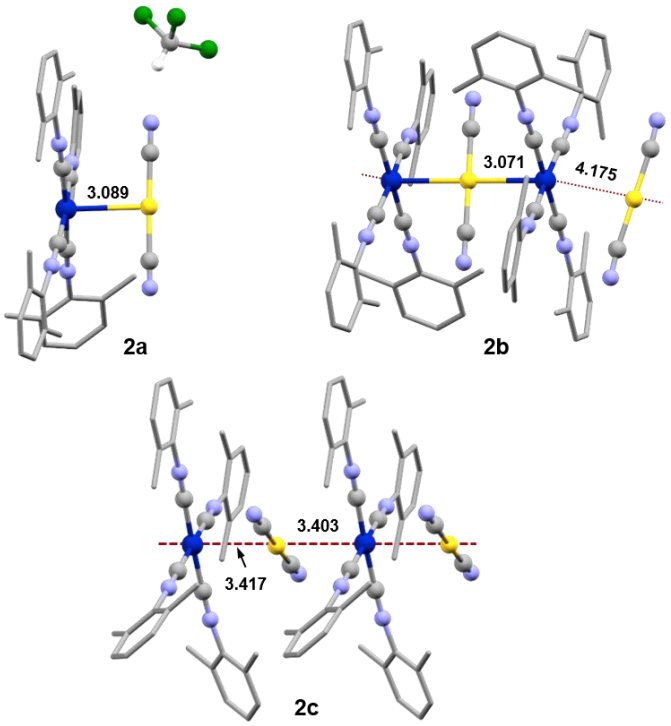

Figure 1. X-Ray structures of orange **2a**, blue **2b** and green **2c**. Rh···Au distances in Å.

[45] (a) Rawashdeh-Omary, M. A.; Omary, M. A.; Patterson, H. H. Oligomerization of $Au(CN)_2^-$ and $Ag(CN)_2^-$ ions in solution *via* ground-state aurophilic and argentophilic bonding. *J. Am. Chem. Soc*. **2000**, *122*, 10371. DOI: 10.1021/ja001545w. (b) Cui, G. L.; Cao, X. Y.; Fang, W. H.; Dolg, M.; Thiel, W. Photoinduced Gold(I)-Gold(I) Chemical Bonding in Dicyanoaurate Oligomers. *Angew. Chem., Int. Ed*. **2013**, *52*, 10281. DOI: 10.1002/anie.201305487.

It is worth noting that, in spite of not being supported by *intra-unit* π-π stacking, $d^8\cdots d^{10}$ interactions totally prevail over their homometallic combinations.[46] We find Au···Rh distances in the range 3.0–3.5 Å, well below the sum of Rh + Au van der Waals radii (4.1–4.7 Å) but also above the sum of covalent radii (2.75 Å). Their competitive formation suggests similar overall stability for the three polymorphs.

At least for the shortest distances, around 3.1 Å, significant orbital overlapping and some contribution to the stability of the crystal can be presumed. However, the main stabilizer factor for the structures is the presence of *inter-unit* π-interactions networks that are impossible to show in Figure 1.

Despite the fact that Rh···Au interactions in our case are not *determining* the structure, but *determined* by the structure, they are the main responsible for the crystal colour. This can be qualitatively understood taking a look to the frontier molecular orbitals (MO) obtained by DFT calculations. The infinite arrangement of **2c** escapes the simple analysis, but representative fragments were selected for **2a** (Rh···Au dimer) and **2b** (Rh···Au···Rh trimer). The X-Ray structures must be maintained and for this reason geometry optimizations were discarded (the fragments are not stable in the gas phase). Figure 2 shows the orbital diagram for **2a**.

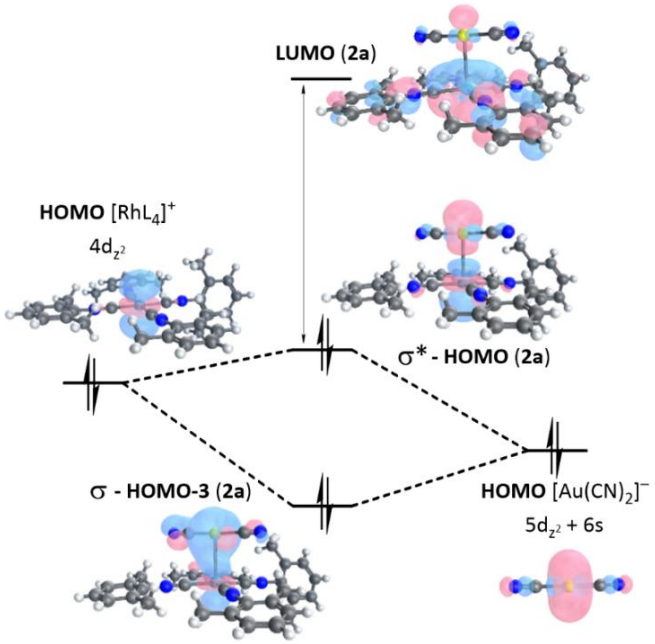

Figure 2. Relevant MOs for the selected fragment of **2a**, and HOMOs of the separated ions.

[46] Similar cases have been reported for $Pt^{II}\cdots Au^{I}$. See for example: Stork, J. R.; Rios, D.; Pham, D.; Bicocca, V.; Olmstead, M. M.; Balch, A. L. Metal−Metal Interactions in Platinum(II)/Gold(I) or Platinum(II)/Silver(I) Salts Containing Planar Cations and Linear Anions. *Inorg. Chem.* **2005**, *44*, 3466. DOI: 10.1021/ic048333a.

The combination of the HOMOs from Rh ($4d_{z2}$) and Au ($5d_{z2}$ + 6s) leads to the bonding σ-HOMO-3 and the antibonding σ*-HOMO, being the later higher in energy and the highest occupied molecular orbital in the fragment. The LUMO has no significant contribution from gold and involves mainly π density from the isocyanide ligands.[43,45] Obviously, the LUMO must be much lower in energy in the real crystal because the stacking interactions are missing in the computational model.

The energy gap HOMO-LUMO determines the colour of the crystal (which is complementary to the absorption in UV-vis spectra). Comparing **2a** (orange) and **2b** (blue), the first must have a smaller gap. The calculations performed with the selected fragments are able to reproduce qualitatively this fact, although they differ in the absolute values due to the oversimplification of the model used for the DFT calculations. The decrease in the energy gap for **2b** is the consequence of the higher destabilization of the σ*-HOMO that is the multiply antibonding combination (of at least 3 metal centres if not five) while the LUMO remains relatively unaltered compared to **2a** (Figure 3). This destabilization of the HOMO has no direct influence in the stability of the crystalline structure because it is concomitantly linked with the stabilization of the bonding combination, but it does determine the colour of the crystal.

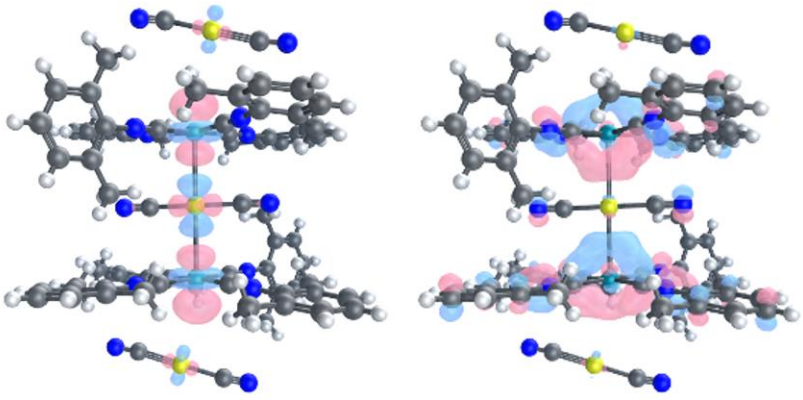

Figure 3. Frontier MOs of a symmetric fragment of **2b**. σ*-HOMO (left) and LUMO (right).

Coming now to the gold(I) isocyanide derivatives and their silver bimetallic analogues, we decided to explore the use of 4-pyridylisocyanide, CN**Py**, to make selectively bimetallic Au/Ag complexes. Initially we obtained the homometallic complexes [AuAr(CNPy)] with Pf (**3**) and Rf (**4**) groups and the heterometallic [{AuAr(CNPy)}$_2$Ag](BF$_4$) (**5** and **6** respectively), with bridging CNPy C-coordinated to Au and N-coordinated to Ag. Neither the free ligand nor the complexes display

luminescence in solution. However, the complexes are luminescent in the solid state, and **3** and **4** display marked mechanochromic behaviour (see Figure 4).[47,48]

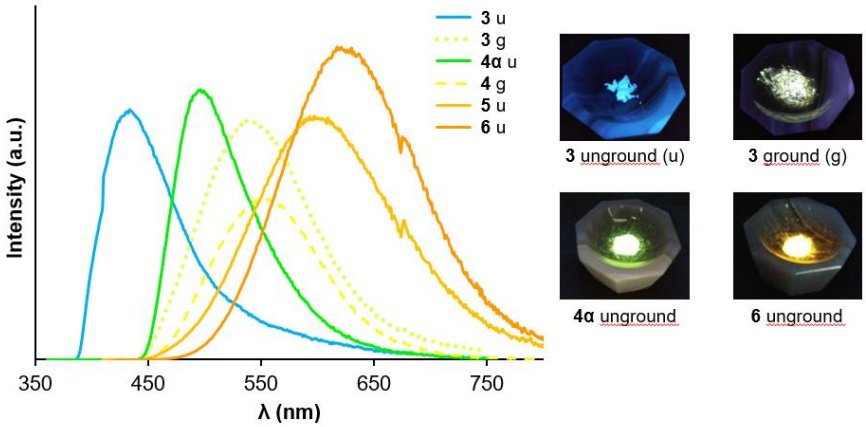

Figure 4. Emission spectra of compounds **3-6** before and after grinding. Photographs taken under irradiation.

In order to rationalize the modifications in the emissions observed in Figure 4, we tried to obtain extra information about the solid structures of these species. Figure 5 gathers the X-Ray molecular structures of **3**, **4** and **6.** In **3**, long Au···Au distances (3.8 Å) are observed and π-stacking seems to direct the packing. The replacement of Pf by Rf in **4** induces a completely different structure with a variety of weak interactions present, halogen···halogen and Au···Au (intermediate distance, 3.3 Å) interactions are added to the ubiquitous stacking. Finally, bimetallic [{AuRf(CNPy)}$_2$Ag](BF$_4$) (**6**) displays very short aurophilic distances (3.1 Å) and direct participation of the silver centre in any metallic interactions is not observed.[49] The structure of **6** clearly shows that the reaction with AgBF$_4$ abruptly modifies the packing of the product due to the steric requirements of the anion.

[47] For reviews see: (a) Sagara, Y.; Yamane, S.; Mitani, M.; Weder, C.; Kato, T. Mechanoresponsive Luminescent Molecular Assemblies: An Emerging Class of Materials. *Adv. Mater*. **2016**, *28*, 1073. DOI: 10.1002/adma.201502589. (b) Xue, P.; Ding, J.; Wang, P.; Lu, R. Recent progress in the mechanochromism of phosphorescent organic molecules and metal complexes. *J. Mater. Chem. C*, **2016**, *4*, 6688. DOI: 10.1039/C6TC01503D.

[48] For one of the first examples of AuAr(CNAr') mechanochromic species see: Ito, H.; Saito, T.; Oshima, N.; Kitamura, N.; Ishizaka, S.; Hinatsu, Y.; Wakeshima, M.; Kato, M.; Tsuge, K.; Sawamura, M. Reversible mechanochromic luminescence of $(C_6F_5Au)_2$(μ-1,4-diisocyanobenzene). *J. Am. Chem. Soc*. **2008**, *130*, 10044. DOI: 10.1021/ja8019356.

[49] For Au^I/Ag^I bimetallic compounds with direct Au···Ag interactions see: Lasanta, T.; Olmos, M. E.; Laguna, A.; Lopez-de-Luzuriaga, J. M.; Naumov, P. Making the Golden Connection: Reversible Mechanochemical and Vapochemical Switching of Luminescence from Bimetallic Gold-Silver Clusters Associated through Aurophilic Interactions. *J. Am. Chem. Soc*. **2011**, *133*, 16358. DOI: 10.1021/ja206845s.

We should not forget the electronic implications of silver that acts as a linker of two AuRf(CNPy) moieties in a trimetallic unit with no dipolar moment.[50]

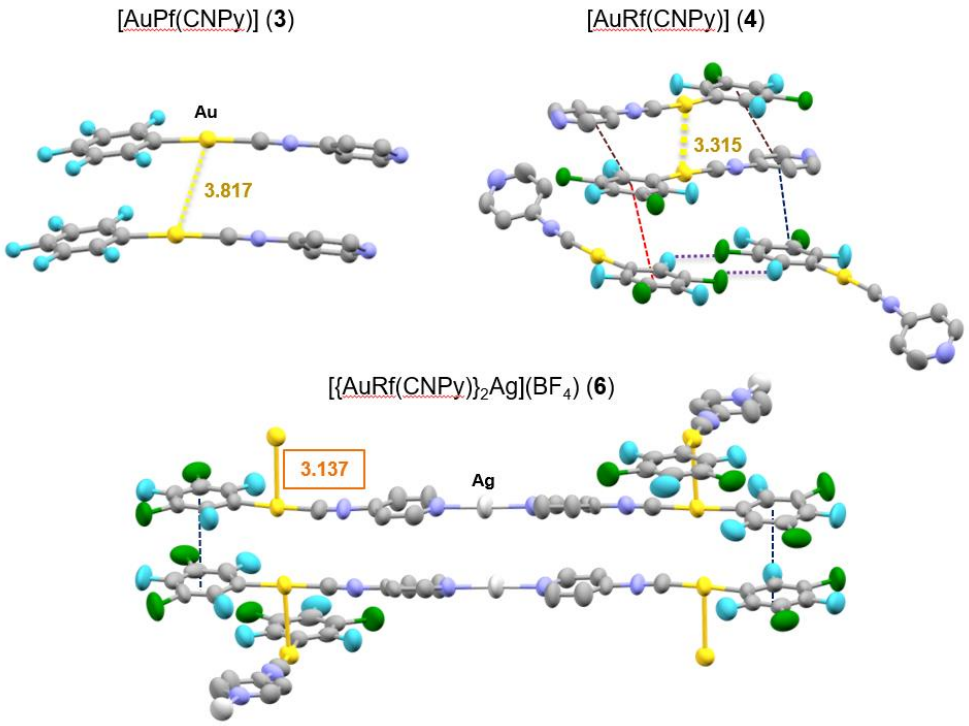

Figure 5. X-Ray structures of **3**, **4** and **6** with Au···Au distances in Å. Dashed lines represent examples of other weak interactions.

The red-shifts in the emission moving from **3** to **4** or from **4** to **6** concur with the shortening in Au···Au distances, and are in agreement with previous works, most of them reported by Ito.[51] Similarly, the mechanochromic behaviour of [AuAr(CNPy] complexes, is a consequence of a loss of crystallinity that leads to amorphous phases with shorter aurophilic interactions.

We also tried to shed light into the orbitals involved in the emission, using in this case TD-DFT calculations. The same restrictions commented above for the Rh···Au system must be applied here in order to maintain the packing. We decided to study the green emitting [AuRf(CNPy)] (**4**) and the orange emitting [{AuRf(CNPy)}$_2$Ag](BF$_4$) (**6**). The later must have a smaller gap because its luminescence is red-shifted. A critical point is

[50] The lack of dipolar moment might preclude the typical antiparallel arrangement: Seki, T.; Kobayashi, K.; Mashimo, T.; Ito, H. A gold isocyanide complex with a pendant carboxy group: orthogonal molecular arrangements and hypsochromically shifted luminescent mechanochromism. *Chem. Commun.* **2018**, *54*, 11136. DOI: 10.1039/C8CC06490C.

[51] Seki, T.; Takamatsu, Y.; Ito, H. A Screening Approach for the Discovery of Mechanochromic Gold(I) Isocyanide Complexes with Crystal-to-Crystal Phase Transitions. *J. Am. Chem. Soc.* **2016**, *138*, 6252. DOI: 10.1021/jacs.6b02409.

the election of simplified fragments that properly represent the solid-structures, and in the case of **6**, silver (and also BF_4) can be spared because they have no significant contribution to the frontier orbitals.

Figure 6 shows the frontier orbitals obtained for fragments of six [AuRf(CNPy)] molecules taken from the X-ray structures of **4** and **6**, and their computed excitation energies. The calculations reflect qualitatively the red-shift observed and also show the main reason for this shift: While the LUMOs in both cases are constituted by π-density of isocyanide ligands, the HOMOs strikingly differ. The gold contribution to the HOMOs is clearly different in both structures: it is negligible in **4** (8%) because the HOMO is located in the Rf moieties, but predominant in **6** (79%). Analogous to the Rh···Au aggregates, the shorter the M···M' distances, the higher the destabilization of the multiple antibonding combination denoted as σ*-HOMO. The consequence of this destabilization is a smaller energy gap and, in this case, a red-shifted emission.

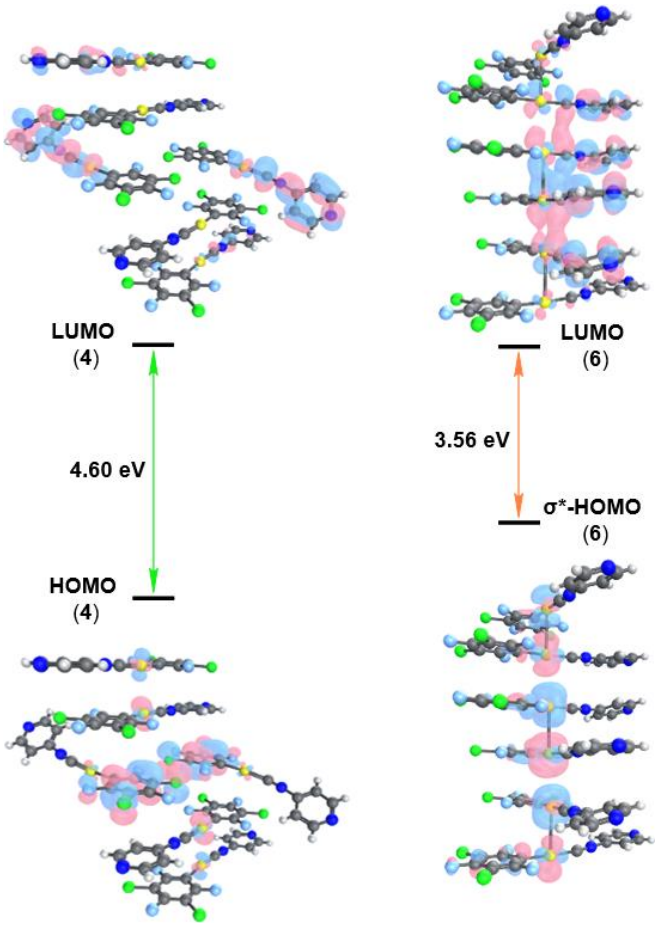

Figure 6. HOMO-LUMO orbitals and TD-DFT excitation energies for selected fragments of **4** (left) and **6** (right)**.**

The most important lesson learned from the detailed study of the different structural data, together with the information obtained from the theoretical calculations presented in this Chapter, is that the crystalline packing is a delicate balance of weak interactions, being the metalophilicity just one more. This is not in contradiction with the fact that these energetically minor M···M' interactions can determine some interesting properties of the material, within the context of an intimate structure-properties relationship. Geometry-restricted DFT studies (at low computational cost) performed over simplified models of the crystal can offer very valuable information, even if sacrificing quantitative accuracy.

Conclusions

Chapter I: *Rh^I/Au^I Transmetalation*

In Rf/Pf exchanges between Rh^I and Au^I complexes the fractional and negative kinetic order in $AsPh_3$ indicates that this transmetalation proceeds *via* a multistep mechanism, one involving ligand dissociation.

In contrast, in the Rf/Cl exchange there is an accelerating effect of $AsPh_3$, which reveals the existence of two cooperative pathways, ligand-catalysed and uncatalysed.

DFT calculations reveal the remarkable tendency for both Rf/Pf and Rf/Cl exchanges to occur via oxidative insertion with formation of heterometallic bonded intermediates.

Chapter II: *RhCp*: Hidden exchanges and buffer effect*

The direct Rf/Pf exchange between 16e [$RhCp^*Ar_2$] species is unfeasible, but proceeds *via* Ar/OH exchanges catalysed by the hydrolysis product $(\mu\text{-}OH)_2[RhCp^*Ar]_2$, present in minute concentrations. The study reveals that these exchanges are efficient and must be operating also when the two aryls are identical.

The synthesis of 18e $[RhCp^*ArCl]_2$ complexes by symmetrization of [$RhCp^*Ar_2$] with $[RhCp^*Cl_2]_2$ is another example of Ar/X exchange, in this case Ar/Cl.

The high stability of the five-coordinate 16e [$RhCp^*Ar_2$] complexes is due to the capability of the Cp* ligand to modulate its electronic donation when needed, diminishing the electronic variations around the metal centre. We call this "*buffer effect of Cp**". The structural analysis of different RhCp* complexes allows us to stablish a series of *trans* influence of ligands in an octahedral environment.

NBO calculations support that in these RhCp* complexes the simple concept of backdonation from metal to π-acceptor ligands needs to be redefined. In fact, non-negligible *lateral donations* from the Cp* to CO or CN^- have to be taken in consideration.

Chapter III: *Reactivity of $PdCl_2$ PEWO-chel Complexes*

$PdCl_2$ is able to coordinate one fluorinated PEWO ligand as chelate and traps the infrequent *Z* configuration of the double bond. The chalcone skeleton of these ligands facilitates the easy *E/Z* isomerization observed.

The *E*/*Z* isomerization triggers a C–F activation process, leading to unreported P-carbene complexes. The proposed aromaticity of these derivatives allows us to rationalize the chemoselectivity of the subsequent reactivity.

These processes must be taken into account as they are a potential complication in new reactions or in catalysis using PEWO ligands.

Chapter IV: *Substoichiometric Protection of Au^I Catalysts*

The substoichiometric protection by $AsPh_3$ of the commonly used $[AuL(W)]^+$ catalysts (W = weakly coordinating ligand) strongly supports a disproportionation mechanism for their decomposition. Stronger ligands, such as PPh_3, cannot play this role because a certain concentration of free ligand is required.

Other silent ligands (superstoichiometric adventitious water is one example) can do the role when the catalyst in decomposition reaches low concentration. This explains the residual activity that remains after massive catalyst decomposition.

Chapter V: *$d^8\cdots d^{10}$ and $d^{10}\cdots d^{10}$ Interactions*

The use of the *ortho*-substituted xylylisocyanide ligand (L) hampers π-π stacking between $[RhL_4]^+$ units preventing $d^8\cdots d^8$ interactions and this helps for the formation in the solid state of $d^8\cdots d^{10}$ interactions with the bimetallic $[RhL_4][Au(CN)_2]$ complex. These metallophilic interactions, although energetically modest, determine the colour of the crystals.

The red shifts in the luminescence observed when modifying the aryl group, incorporating silver or grinding, both in homometallic [AuAr(CNPy)] and in bimetallic $[\{AuAr(CNPy)\}_2Ag]BF_4$ complexes, are intimately related with the formation of shorter aurophilic interactions in the solids.

Geometry restricted DFT and TD-DFT calculations, using representative fragments of the crystalline structures, allow to identify the orbitals involved in these photophysical properties.

General conclusions

The different and diverse topics dealt with in this PhD work highlight the power of combining experimental and theoretical tools when facing chemical problems, not only in the field of mechanistic studies but also in the planning and understanding of other areas, such as the production of deeply coloured or luminescent materials in our case.

On the other, the easy accessibility to collections of data, harder to get at the time when some chemical concepts were defined (*trans* influence, σ-donation + π-backdonation…), offers an opportunity to look at them in a non-routine way and get a deeper understanding of their significance and applicability.

Methods

The methodology used in this thesis is familiar to all the researchers in chemistry at this level of exigence. Herein, I will describe only the general methods while the particular details, including the characterisation of the new compounds, are collected in the Supplementary Information of the scientific articles.

The reactions were performed under N_2 atmosphere. Solvents were purified according to standard procedures. ^{1}H, $^{13}C\{^{1}H\}$, ^{19}F and $^{31}P\{^{1}H\}$ NMR spectra were recorded on Bruker AV–400 or Varian 500/54 Premium Shielded instruments. In the spectra registered in non-deuterated solvents, a coaxial tube containing acetone-d_6 was used to maintain the ^{2}H lock signal. Infrared spectra were recorded with Perkin–Elmer Frontier (4000–200 cm^{-1}) equipped with an ATR accessory (*Attenuated Total Reflection*) for the direct recording of solid samples. The elemental analyses were performed with a Carlo Erba 1108 microanalyser (by Vigo University, Spain).

Kinetic experiments were monitored by ^{19}F or ^{1}H NMR. The reagents, the solvent and the internal reference (when needed) were added in an NMR tube and placed into a thermostated probe in a NMR apparatus. The temperature of the sample was determined using methanol as chemical shift thermometer. Concentration-time data were then acquired from the integrals of the selected signals. Linear fittings afforded initial rates. The kinetic models were fitted to the measured concentration *vs.* time experimental data by nonlinear least-squares (NLLS) regression, using the Program COPASI.

For the X-ray diffraction studies, the crystals were attached to a glass fiber or a micromount and transferred to an Agilent Supernova diffractometer with an Atlas CCD area detector. Data collection was performed with Mo-Kα radiation (λ = 0.71073 Å) or Cu-Kα (λ = 1.54184 Å). Data integration, scaling and empirical absorption correction was carried out using the CrysAlisPro program package. Using Olex2, the structure was solved with the ShelxT, and refined with ShelxL program.

Density functional theory (DFT) calculations reported in this work were carried out using the dispersion corrected hybrid functional ωB97X-D. C, P, As and H atoms were described using the double-ζ basis set 6-31G(d,p), whereas the same basis set plus diffuse functions was employed to describe the more electronegative O, N, Cl and F atoms. Transition metals were described using the effective core potential LANL2DZ including f-polarization functions. Geometry optimizations in vacuum were performed without

imposing any constraint and the nature of all the stationary points was further verified through vibrational frequency analysis. For transition states, geometry relaxations along the reaction coordinate were also carried out to confirm they connect the corresponding reaction energy minima. The effect of the solvent employed in the experiments was introduced through single-point calculations at the optimized geometries in vacuum using the SMD solvation model. Selected bonding interactions were studied by means of natural bond orbital (NBO) and second-order perturbation theory (SOPT) analyses. In the cases collected in Chapter V, geometry optimizations were discarded and we respected the X-ray obtained structures.

List of Publications

At the time of the completion of the memory, the results summarised in this thesis have led to eight scientific articles and one manuscript to be submitted soon. Only the final parts of Chapters I and II are unpublished.

The studies of Chapter V have been carried out in collaboration with another Ph. D student and are excluded from the compendium.

***Article I** (Chapter I)*

$Rh^{I}Ar/Au^{I}Ar'$ Transmetalation: A Case of Group Exchange Pivoting on the Formation of M–M' Bonds through Oxidative Insertion

Peñas-Defrutos, M. N.; Bartolomé, C.; García-Melchor, M.; Espinet, P. *Angew. Chem. Int. Ed.* **2019**, *58*, 3501. DOI: *10.1002/anie.201813419*.

Abstract: By combining kinetic experiments, theoretical calculations, and microkinetic modeling, we show that Pf/Rf ($C_6F_5/C_6Cl_2F_3$) exchange between [AuPf($AsPh_3$)] and *trans*-[RhRf(CO)($AsPh_3$)$_2$] does not occur by typical concerted Pf/Rf transmetalation via electron-deficient double bridges. Instead, it involves asymmetric oxidative insertion of the Rh^{I} complex into the (Ph_3As)Au–Pf bond to produce a [(Ph_3As)Au–RhPfRf(CO)($AsPh_3$)$_2$] intermediate, followed by isomerization and reductive elimination of [AuRf($AsPh_3$)]. Interesting differences were found between the LAu–Ar asymmetric oxidative insertion and the classical oxidative addition process of H_2 to Vaska complexes.

***Manuscript II** (Chapter I)*

Accelerating Effect of $AsPh_3$ in the Rh^I/Au^I Transmetalation. Reversible Tricoordination of Au^I Eases its Oxidative Insertion in the Rh–C Bond

Peñas-Defrutos, M. N.; Bartolomé, C.; García-Melchor, M.; Espinet, P. *Manuscript in preparation* (Attached at the end of the document).

Abstract: The Ar/Cl (Ar = $C_6Cl_2F_3$-3,5) exchange between [AuClL] (L = $AsPh_3$) and *trans*-[RhAr(CO)L_2] is accelerated by addition of an excess of L. By combining experimental data, DFT simulations and microkinetic modeling, we demonstrate the existence of two competitive pathways. The addition of L has a catalytic effect and opens a mechanism involving the coordination of the additional L giving a tricoordinate [AuClL_2] species, which transmetalates faster compared to the linear analogue [AuClL]. Instead of involving double-bridged transition states, both mechanisms involve the initial oxidative insertion of Au into the Rh–C bond to afford intermediates with strong metal-metal bonds.

Article III *(Chapter II)*

Hidden aryl-exchange processes in stable 16e Rh^{III} [RhCpAr_2] complexes, and their unexpected transmetalation mechanism*

Peñas-Defrutos, M. N.; Bartolomé, C.; García-Melchor, M.; Espinet, P. *Chem. Commun.* **2018**, *54*, 984. DOI: *10.1039/c7cc09352g*.

Abstract: Experiments mixing the stable 16e 5-coordinate complexes [RhCp*Ar_2] (Cp* = C_5Me_5; Ar = C_6F_5, $C_6F_3Cl_2$-3,5) uncover fast aryl transmetalations. Unexpectedly, as supported computationally, these exchanges are not spontaneous, but catalyzed by minute amounts of 18e (μ-OH)$_2$[RhCp*Ar]$_2$ as a source of 16e [RhCp*Ar(OH)]. The OH group is an amazingly efficient bridging partner to diminish the activation barrier of transmetalation.

Article IV *(Chapter II)*

*Coordinatively Unsaturated [RhCp*Rf$_2$] (Cp* = C$_5$Me$_5$; Rf = C$_6$F$_3$Cl$_2$-3,5), General Precursor to Cp*-Diaryl and Cp*-Halo-Aryl Rh^{III} Complexes. Observing and Testing the Effect of Cp* as Electronic*

Peñas-Defrutos, M. N.; Bartolomé, C.; Espinet, P. *Organometallics* **2018**, 37, 3533. DOI: *10.1021/acs.organomet.8b00227*.

Abstract: The pentacoordinated [RhCp*Rf$_2$] (Rf = C$_6$F$_3$Cl$_2$-3,5) and the octahedral (μ-Cl)$_2$[RhCp*Rf]$_2$, obtained by stoichiometric rearrangement with (μ-Cl)$_2$[RhCp*Cl]$_2$, are general precursors of [RhCp*RfXL] (X = Rf, Cl; L = ligand) complexes, which were studied by NMR (L dissociation and fluxional processes) and X-ray diffraction (structural effects affecting the Rh–Cp* distances) techniques. The Rh–Cp*$_{centroid}$ distances decrease markedly for identical L in the order [RhCp*Rf$_2$L] > [RhCp*RfClL] > [RhCp*Cl$_2$L] and are further influenced regularly within each family by the *trans influence* of L (longer distances for higher trans influence of L). The structural effects observed reveal a remarkable capability of Cp* to act as an electron-density buffer, which attenuates the Rh electron density variations induced by the substituents in front of Cp* by releasing toward Rh or polarizing toward Cp*, on demand, the electron density of the Rh–Cp* bonds. This *buffer effect* explains the easy L dissociation from [RhCp*Rf$_2$L] and the accessibility to formally 16e pentacoordinated [RhCp*Rf$_2$].

***Article V** (Chapter III)*

E−Z Isomerization of Phosphine-Olefin (PEWO-F$_4$) Ligands Revealed upon PdCl$_2$ Capture: Facts and Mechanism

Peñas-Defrutos, M. N.; Vélez, A.; Gioria E.; Espinet, P. *Organometallics* **2019**, 38, 4701. DOI: *10.1021/acs.organomet.9b00679*.

Abstract: The PEWO phosphines R$_2$P(*o*-C$_6$H$_4$CH=CHC(O)Ph), R$_2$P(*o*-C$_6$H$_2$F$_2$CH=CHC(O)Ph), and R$_2$P(*o*-C$_6$F$_4$CH=CHC(O)Ph) and their P-monodentate complexes *trans*-[PdCl$_2$(P-monodentate)$_2$] show, in solution and (when available) in the X-ray diffraction structures, an *E* configuration of the double bond. In contrast, the structures of [PdCl$_2$(P-chelate)] display *E* and *Z* configurations. The *E/Z* isomerization of the latter requires first decoordination of the double bond, which then allows for easy rotation about the electron-deficient double bond. Thus, the *E/Z* equilibria exist for the free and the P-monodentate complexes as well but are not observed because they are extremely displaced toward the *E* isomer. Their capture in the form of [PdCl$_2$(P-chelate)], with equilibrium constants on the order $K_{eq} \approx 1–3$, allows the two configurations to be observed and isolated. Evaluation of their ability to couple Pf–Pf from *cis*-[PdPf$_2$(THF)$_2$] (Pf = C$_6$F$_5$) affords values of their $\Delta G^{\ddagger}(\text{Pf–Pf})_{Pd}$ parameters confirming that higher substitution of H by F produces lower coupling barriers and a double bond that is more electron deficient when it is free and more electron withdrawing when it is coordinated.

***Article VI** (Chapter III)*

Reactivity of Fluorinated-Chalcone Phosphines, RPEWO-F_4, Induced by C−F Activation upon Coordination to $PdCl_2$

Peñas-Defrutos, M. N.; Vélez, A.; Espinet, P. *Organometallics* **2020**, 39, 841. DOI: *10.1021/acs.organomet.0c00019*.

Abstract: The *E* phosphine ligands (R = Ph, *o*-Tol, Cy), abbreviated as RPEWO-F_4, are stable in solution, but they develop a rich reactivity on coordination to $PdCl_2$. The chelate P-olefin coordination to $PdCl_2$ leads eventually to a *Z* conformation of the fluorinated-chalcone group *o*-$C_6F_4CH{=}CHC(O)Ph$. From there, a cyclization reaction occurs involving the C=O group and activation of a F atom, yielding a strongly chelated [$PdCl_2$(P-carbene)] complex. The carbene carbon atom in the complex displays some electrophilicity, which is expressed in hydrolysis, ammonolysis, and oxidation (with peroxide) reactions, affording $PdCl_2$ complexes with new P,C,O-pincer, P,C,N-pincer, or P,O-chelate fluorinated ligands. The C–F activation reactions are slow in comparison to the catalysis rates when the [$PdCl_2$(RPEWO-F_4)] complexes have been used in Negishi catalyses. Consequently, the reactivity discussed here is not expected to interfere with the interpretation of the data obtained in Pd-catalytic studies or processes, at least for fast transmetalating nucleophiles.

Article VII *(Chapter IV)*

Some Singular Features of Gold Catalysis: Protection of Gold(I) Catalysts by Substoichiometric Agents and Associated Phenomena

Bartolomé, C.; Ramiro, Z.; Peñas-Defrutos, M. N.; Espinet, P. *ACS Catal.* **2016**, *6*, 6537. DOI: *10.1021/acscatal.6b01825*.

Abstract: This study deals with two striking phenomena: the complete protection against decomposition of hypothetically monocoordinated Au^{I} intermediates [AuL]Y (L = strongly coordinating ligand; Y^- = poorly coordinating anion) by addition of small substoichiometric amounts (5 mol % relative to Au) of not strongly coordinating ligands (e.g., $AsPh_3$) and the fact that, in contrast, strongly coordinating ligands cannot provide this substoichiometric protection. The two phenomena are explained considering that (*i*) the existence of real monocoordinated [AuL]Y is negligible in condensed phases and the kinetically efficient existing species are dicoordinated [AuL(W)]Y (W = any very weakly coordinating ligand existing in solution, including OH_2, the solvent, or the Y^- anion) and (*ii*) these [AuL(W)]Y intermediates give rise to decomposition by a disproportionation mechanism, via polynuclear intermediates formed by associative oligomerization with release of some W ligands. It is also shown that very small concentrations of [AuL(W)]Y are still catalytically efficient and can be stabilized by overstoichiometric adventitious water, so that full decomposition of the catalyst is hardly reached, although eventually the stabilized concentration can be kinetically inefficient for the catalysis. These results suggest that, in cases of gold catalysis requiring the use of a significant quantity of gold catalyst, the turnover numbers can be increased or the concentration of gold catalyst widely reduced, using substoichiometric protection properly tuned to the case.

Article VIII *(Chapter V)*

$d^8\cdots d^{10}$ $Rh^I\cdots Au^I$ interactions in Rh 2,6-xylylisocyanide complexes with $[Au(CN)_2]^-$: bond analysis and crystal effects

Conejo-Rodríguez, V.; Peñas-Defrutos, M. N.; Espinet, P. *Chem. Commun.* **2019**, *55*, 5005. DOI: *10.1039/c9cc01377f*.

Abstract: The well-known $[RhL_4]_n(anion)_n$ structures, with $Rh^I\cdots Rh^I$ $d^8\cdots d^8$ interactions, are replaced by others with $Rh^I\cdots Au^I$ $d^8\cdots d^{10}$ interactions such as $[\{RhL_4\}\{Au(CN)_2\}]$ (L = 2,6-xylylisocyanide) or $[\{RhL_4\}\{Au(CN)_2\}\{RhL_4\}\{Au_2(CN)_3\}\cdot 4(CHCl_3)]_\infty$ when the anion is $[Au(CN)_2]^-$. Orbital (Rh···Au), coulombic, and inter-unit π–π aryl stacking interactions stabilize these crystal structures.

Article IX *(Chapter V)*

4-Pyridylisocyanide gold(I) and gold(I)-plus-silver(I) luminescent and mechanochromic materials: the silver role

Conejo-Rodríguez, V.; Peñas-Defrutos, M. N.; Espinet, P. *Dalton Trans.* **2019**, *48*, 10412. DOI: *10.1039/c9dt01618j*.

Abstract: Crystallographic and DFT examination of the metalloligands [AuAr(CNPy)] (Ar = C_6F_5 (**1**), $C_6F_3Cl_2$-3,5 (**2**)) and their silver complexes [Ag[AuAr(CNPy)]$_2$](BF_4) (**3** and **4**) support that the marked luminescence red-shifts observed on moving from **1** to **2**, from **1**,**2** to **3**,**4**, or upon grinding, are not caused by electronic differences (either by changing the aryls C_6F_5/$C_6F_3Cl_2$, or by N coordination to silver), nor by non-existent Au···Ag interactions. They are always due to structural changes disturbing stronger π–π stackings in order to allow for shorter Au···Au interactions.

Accelerating Effect of $AsPh_3$ in the Rh^I/Au^I Transmetalation. Reversible Tricoordination of Au^I Eases its Oxidative Insertion in the Rh–C Bond

Marconi N. Peñas-Defrutos,[a] Camino Bartolomé,*[a] Max García-Melchor,*[b] and Pablo Espinet*[a]

Abstract: The Ar/Cl (Ar = $C_6Cl_2F_3$-3,5) exchange between [AuClL] (L = $AsPh_3$) and *trans*-[RhAr(CO)L_2] is accelerated by addition of an excess of L. By combining experimental data, DFT simulations and microkinetic modeling, we demonstrate the existence of two competitive pathways. The addition of L has a catalytic effect and opens a mechanism involving the coordination of the additional L giving a tricoordinate [AuClL_2] species, which transmetalates faster compared to the linear analogue [AuClL]. Instead of involving double-bridged transition states, both mechanisms involve the initial oxidative insertion of Au into the Rh–C bond to afford intermediates with strong metal-metal bonds.

Bimetallic catalysis[1] refers to homogeneous processes in which two transition metals (TM), or one TM and one group-11 element (M), [2] cooperate in a synthetic transformation (often C−C coupling) and their actions are linked by a transmetalation step. The understanding of transmetalation mechanisms in this recent area may help in the design of efficient catalytic systems (see for instance the gold assisted Stille type couplings for bulky aryls).[3,4] The cooperativity of Pd^{II}/Au^I and Pd^{II}/Cu^I pairs (e.g. the Sonigashira reaction) has been reasonably studied in the past. The lack of mechanistic studies on the promising Rh^I/Au^I dyad prompted us to investigate their transmetalation possibilities, and very recently we reported the aryl scrambling between the Vaska-type complex *trans*-[RhRf(CO)($AsPh_3$)$_2$] (Rf = $C_6F_3Cl_2$-3,5) and [AuPf($AsPh_3$)] (Pf = C_6F_5).[5] We discovered that, instead of the classical transmetalation mechanism featuring a double aryl bridged transition state, the aryl exchange occurred unexpectedly *via* oxidative insertion of rhodium into the Au–C bond (Figure 1). [6] The fluorinated-aryls facilitate ^{19}F NMR monitoring, providing valuable kinetic information to elucidate the transmetalation mechanism. [7] In that study, the unconventional fractional and negative kinetic dependence upon free ligand addition ($AsPh_3$ slows down that reaction) revealed an entangled mechanism. Only combining kinetics, density functional theory (DFT) calculations, and microkinetic modelling, could the complete pathway be established as a reversible process involving oxidative insertion, ligand dissociation and isomerization steps, laying very close in energy. [8]

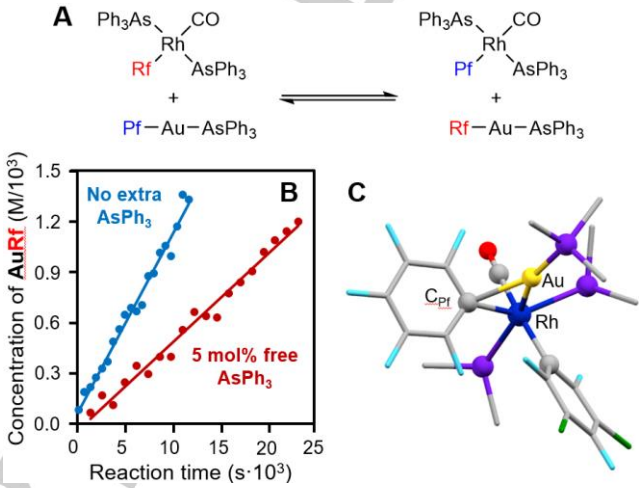

Figure 1. A) Reversible aryl exchange between *trans*-[RhRf(CO)($AsPh_3$)$_2$] and [AuPf($AsPh_3$)]. **B**) Ligand effect on the initial transmetalation rate. **C**) Transition state leading to Rh insertion into the Au–C_{Pf} bond. An octahedral intermediate with a Rh–Au bond is formed. Ph groups in the arsine are omitted for clarity.

The most frequently desired exchange in catalysis is R for X (R = organic group; X = halide), in order to bring the R group to the catalytic transition metal. It is worth noting that the mechanistic differences between R/R' and R/X exchanges, even when using the same metal combination, can be striking. For instance, for Au^I/Sn^{IV} exchanges the double bridges mechanism was found in the Ph/Cl exchange, whereas the Ph/vinyl transmetalation followed an oxidative addition/reductive elimination (OA/RE) pathway via an intermediate with an Au–Sn bond.[9]

Here we report a thorough thermodynamic, kinetic, and DFT investigation of the Rf/Cl exchange in (Eq. 1), where the square-planar complex *trans*-[RhRf(CO)($AsPh_3$)$_2$] (**1**) and the linear complex [AuCl($AsPh_3$)] (**2**) lead to the products *trans*-[RhCl(CO)($AsPh_3$)$_2$] (**3**) and [AuRf($AsPh_3$)] (**4**). The aryl Rf is chosen for simplicity of its ^{19}F NMR signals, and the Rh complex because the high preference of CO for the *trans* position to Rf or Cl avoids the formation of other isomers. Au and Rh complexes with the same neutral ligand ($AsPh_3$) are used to prevent multiplication of signals due exclusively to ligand exchanges.

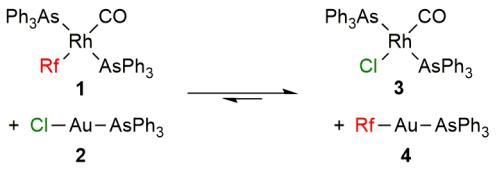

(1)

In the case studied here, the exchange equilibrium is highly displaced to formation of [AuRf($AsPh_3$)] (**4**) and *trans*-[RhCl(CO)($AsPh_3$)$_2$] (**3**). [10] The exchange in stoichiometric conditions (1:1 molar ratio) was monitored in CD_2Cl_2 in both senses until steady concentrations of the species were reached

[a] Mr. Marconi N. Peñas-Defrutos, Dr. Camino Bartolomé, and Prof. Dr. Pablo Espinet.
IU CINQUIMA/Química Inorgánica, Facultad de Ciencias, Universidad de Valladolid, 47071-Valladolid (Spain).
E-mails: caminob@qi.uva.es and espinet@qi.uva.es
[b] Prof. Max García-Melchor
School of Chemistry, CRANN and AMBER Research Centres, Trinity College Dublin, College Green, Dublin 2, Ireland. E-mail: garciamm@tcd.ie
Supporting information for this article is given via a link at the end of the document.

(24 h at room temperature), affording K_{eq} = 7×10^3 (ΔG_0 = –5.2 kcal mol^{-1}). This equilibrium constant corresponds to 99% conversion (Figure SX), which would allow, for a simpler kinetic fitting, handling the exchange as an irreversible process with sufficiently good approximation.

The reaction **1**+**2** in CD_2Cl_2 has an appropriate rate for very precise ^{19}F NMR monitoring at 273 K, and the initial rates method can be applied.[11] The integrals of well-separated F_{ortho} signals of species **1** and **4** were monitored. Neither by-products nor reaction intermediates were detected. Least squares adjustment of the data (Figure 2, orange line) yielded an initial reaction rate r_0 = 2.11×10^{-7} mol L^{-1} s^{-1}, corresponding to $\Delta G^{\ddagger}_{273K}$ = 19.3 kcal mol^{-1} for the overall process (for details, see kinetic section in the SI). This Rh to Au Rf/Cl exchange is remarkably faster than the Rf/Pf scrambling studied before.[5] Experiments using 2:1 or 1:2 Au:Rh ratios, doubled the rate of the stoichiometric reaction, confirming first order reaction kinetics in both reactants. Finally, in striking contrast with the Rf/Pf exchange, which showed high deceleration with small percentages of $AsPh_3$ added, the addition of free $AsPh_3$ to Eq. 1 accelerates the transmetalation (Figure 2).

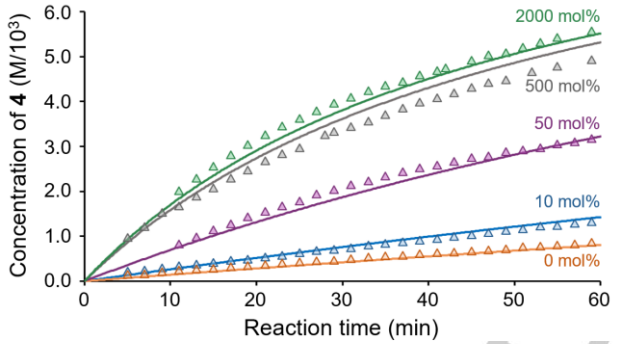

Figure 2. Concentration *vs* time data (triangles) obtained by monitoring the formation of the product [AuRf($AsPh_3$)] (**4**) by means of ^{19}F NMR in CD_2Cl_2 at 273 K with different amounts of free ligand added. Initial concentrations of the reactants: $[Rh]_0 = [Au]_0$ = 1.0 × 10^{-2} mol×L^{-1}. Lines represent data adjusted with COPASI software.

As shown in Figure 2, even substoichometric amounts of ligand result in a noticeable increase in the reaction rate. More specifically, the addition of 10 mol% $AsPh_3$ relative to gold concentration accelerates the transmetalation rate by *ca.* 60% (blue line), while a four-fold increase in the initial rate compared to the reaction in the absence of additional $AsPh_3$ (orange line) is observed with 50 mol% of ligand (violet line). The reaction rate increases further when moving to superstoichometric amounts of ligand, although the observed correlation is not linear, *i.e.* the experiment with 500 mol% $AsPh_3$ is only *ca.* 60% faster than with 50 mol% (see Table SX for details). Hence, the transmetalation rate seems to level off at high ligand concentrations as we can see comparing grey and green lines. These experiments support that, different to the case of Rf/Pf exchange, there is no $AsPh_3$ dissociation involved. On the contrary they suggest the existence of two competing reaction pathways: one that has no participation of the added $AsPh_3$ ligand (Pathway A), and a second one with a lower activation energy, in which $AsPh_3$ participates (Pathway B). For the latter a reasonable proposal is that some added arsine coordinates to gold, makes it more prone to oxidation, and is released after the transmetalation. Consequently, it is in fact an $AsPh_3$ catalyzed process. Both mechanisms lead to formation of the same species and are connected by a coordination equilibrium constant. In order to achieve a fine adjustment of the experimental data we have carried out kinetic simulations with COPASI software.[12] The kinetic model summarized in Scheme 1, fits well the experimental data (lines in Figure 2) both in the absence and presence of additional concentrations of $AsPh_3$ ligand (see SI for details).

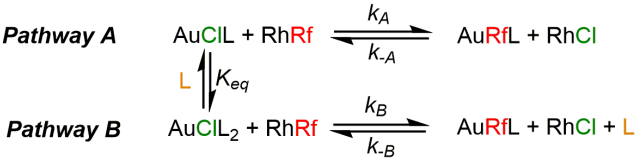

Scheme 1. Kinetic model for COPASI fitting.

Without extra ligand only pathway A is operating, with a COPASI adjusted activation energy barrier value of $\Delta G_A^{\ddagger}$ = 19.2 kcal mol^{-1}. A crucial aspect to be modelled upon addition of $AsPh_3$ is the equilibrium constant to form the active [AuCl($AsPh_3$)$_2$], which determines the amount tricoordinate species formed depending on the of arsine added. The saturation observed when large amounts of ligand are added (5 and 20 eq, Figure 2) suggests substantial contribution of Pathway B, and the adjustment leads to $\Delta G_B^{\ddagger}$ = 17.7 kcal×mol^{-1} (see SI for details).

We conducted a mechanistic investigation of the two competing reaction pathways by means of density functional theory (DFT) calculations at the wb97xd level (see SI for details). The Gibbs energy profile obtained for the uncatalyzed Pathway A is shown in Figure 3.

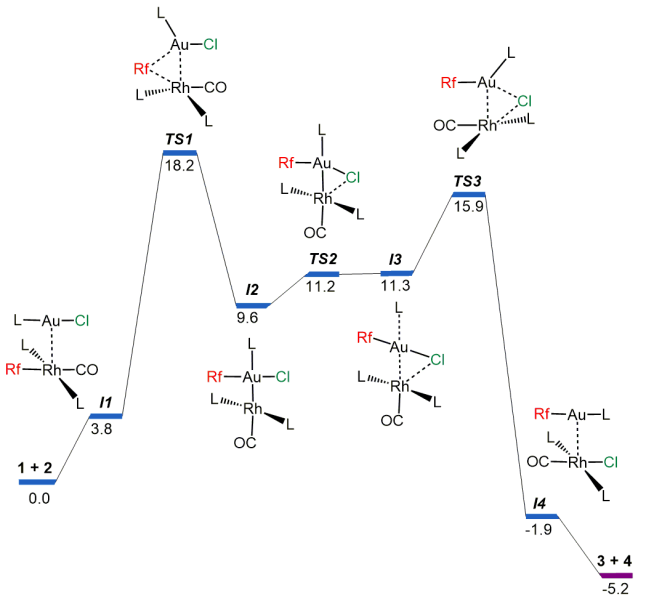

Figure 3. Gibbs energy diagram (in kcal mol^{-1}) for the transmetalation reaction between **1** and **2** in CH_2Cl_2 (Pathway A).

The first step involves the interaction of complexes **1** and **2** to yield a weakly bound Van der Waals complex (***I1***), which lies 3.8 kcal mol^{-1} above the separated reactants. From this intermediate, the oxidative insertion of the Au center into the Rh–C bond takes place via the transition state ***TS1***, requiring an overall activation energy of 18.2 kcal mol^{-1}. This step results in the formation of the reaction intermediate ***I2***, wherein both metal centers display square planar geometries characteristic of Au^{III} and Rh^{I} complexes. Subsequently, the transmetalation of the Cl group occurs in a stepwise process which involves two transition states (***TS2*** and ***TS3***) of relatively low energy. In particular, ***TS2*** entails the formation of an Au–Cl–Rh bridge with a relative barrier of only 1.6 kcal mol^{-1} leading to the intermediate ***I3***, which features substantial labilization of the $AsPh_3$ coordinated to gold. Finally, the Au–Cl bond cleavage takes place via ***TS3*** to afford the intermediate ***I4***. This last intermediate is analogous to ***I1*** but with the reaction products *trans*-[RhCl(CO)($AsPh_3$)$_2$] (**3**) and [AuRf($AsPh_3$)] (**4**) formed. The rate determining step corresponds to the oxidative insertion (***TS1***) with an activation energy that matches very well with the experimental kinetic studies (18.2 *vs* 19.2 kcal×mol^{-1}, respectively.)

To gain a better understanding of the oxidative insertion step, in the following we analyze the optimized structures of ***TS1*** and ***I2*** (Figure 4) in detail.

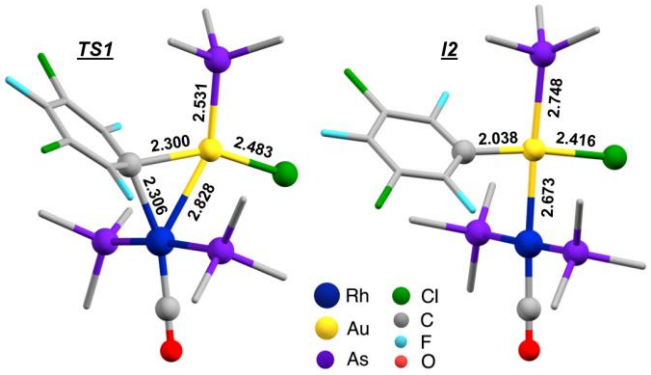

Figure 4. Balls and sticks optimized structures of ***TS1*** (left) and ***I2*** (right) with selected bond distances (Å). Ph groups of the $AsPh_3$ ligands are omitted for clarity. **Sum of covalent radii**: Au-Rh = 2.78 Å; Au-C = 2.09 Å; Rh-C = 2.15 Å; Au-As = 2.55 Å; Au-Cl = 2.38 Å.[13]

Interestingly, while the Rf group acts as a bridging group between both metals in ***TS1*** (with typical M–C$_{ipso}$ distances *ca.* 2.3 Å), the Cl behaves as a mere spectator and remains coordinated to gold. Hence, the sequential formation of one bridge with strong Au–Rh interaction (2.828 Å in ***TS1***) results to be more feasible than the exchange *via* mixed doubled bridges, which precludes this type of metallophilic interactions. Similarly, the resulting intermediate, ***I2***, features an Au–Rh bond with an intermetallic distance comparable to that found by X-Ray diffraction in an heterobimetallic complex, (*i.e.* 2.673 and 2.690 Å, respectively).[14] Moreover, a noticeably elongation of the Au–As is observed in ***I2***, which can be attributed to the very large *trans influence* of the Au–Rh bond.[5]

Coming back to the $AsPh_3$ accelerating effect, it must be the consequence of the existence of an uncovered associative process. We also note that the ^{19}F NMR spectra recorded either from *trans*-[RhRf(CO)($AsPh_3$)$_2$] (**1**) or [AuRf($AsPh_3$)] (**4**) did not show any noticeable change in the chemical shifts upon the addition of a large excess of free $AsPh_3$ ligand, which rules out these species as the origin of the ligand dependence.

Despite the fact that gold(I) tendency to linear coordination is much higher than that of other M(I) coinage metals, there are some examples in the literature of trigonal planar or pseudotetrahedral Au^{I} complexes.[15] For example, the reaction of [AuCl(PPh_3)] with an excess of PPh_3 in polar solvents has been shown to form [AuCl(PPh_3)$_n$] with n = 2 or 3.[16] Notably, the X-Ray structure of the four-coordinate [AuCl(PPh_3)$_3$] shows a clear deviation from tetrahedral geometry with a very long Au···Cl distance (2.71 Å *vs* 2.28 Å in the linear [AuCl(PPh_3)]) which resembles an ion pair. Similar multiple coordination equilibria might also occur with an excess of $AsPh_3$. In fact, [AuX($AsPh_3$)$_m$] structures (X = halide; m = 1, 2, 3,) have been reported, featuring a progressive elongation of the Au–X bond upon coordination of additional ligands.[17] Even the formation of the tetrahedral complex [Au($AsPh_3$)$_4$]$^+$ can be achieved with a non-coordinating counteranion such as BF_4^-.[18]

In our case, the formation of [AuCl($AsPh_3$)$_2$] under reaction conditions (CH_2Cl_2) was confirmed by mass spectrometry, even in the presence of substoichoimetric amounts of added ligand (exact mass of Au($AsPh_3$)$_n$ for n = 2 was observed, while the aggregate with n = 3 was not. See SI for details). These findings are in agreement with DFT calculations, which predict a Gibbs reaction energy of –1.1 kcal×mol^{-1} in CH_2Cl_2 for the formation of [AuCl($AsPh_3$)$_2$] (**5**) from **2** and $AsPh_3$, pointing to an equilibrium between these species. With this knowledge, we set out to model the transmetalation mechanism for the $AsPh_3$-promoted Rf–Cl exchange (Pathway B) starting from the three-coordinate Au complex **5** and the Rh complex **1**. The Gibbs energy profile obtained for this exchange is shown in Figure 5.

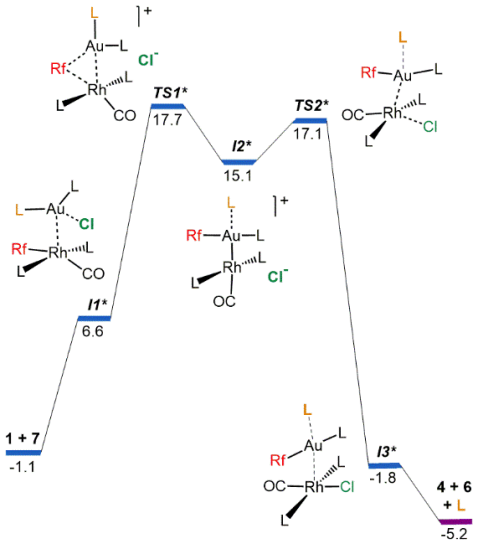

Figure 5. Gibbs energy diagram (in kcal mol^{-1}) for the ligand-promoted transmetalation between **1** and **5** (Pathway B) in CH_2Cl_2.

Similarly, to the uncatalyzed mechanism (Figure 3), the first step in the $AsPh_3$-catalized pathway involves the formation of the Van

der Waals complex between **1** and **5**, followed by the oxidative insertion of Au into the Rh–C_{Rf} bond through ***TS1****. Importantly, this transition state represents the rate determining step of the process, requiring an activation energy barrier of 18.8 kcal mol^{-1} and features the Rf ligand as the only bridging group and a rather short Au–Rh distance (*i.e.* 2.820 Å), despite the bulky environment created by the four $AsPh_3$ ligands. Furthermore, the additional $AsPh_3$ ligand in ***TS1**** (highlighted in orange in Figure 5) remains coordinated to Au, while the Cl group is completely dissociated (highlighted in green) and interacting with several CH groups from the $AsPh_3$ ligands (see SI for the structures of TSs and intermediates with relevant distances). Hence, both ***TS1**** and the resulting intermediate ***I2**** are better described as ion pair species. The latter also displays a noticeably elongation of the Au–As bond in *trans* to Rh, which undergoes complete dissociation with the concomitant formation of the Rh–Cl bond via ***TS2****. This last step requires a relative barrier of only 2.0 kcal mol^{-1} and leads to the intermediate ***I3****, wherein the transmetalated products **3** and **4** are weakly interacting and the additional $AsPh_3$ ligand has been regenerated to participate in the next catalytic cycle.

The computed values for the overall activation energy barriers for both pathways are practically the same (18.2 *vs* 18.8 kcal mol^{-}1). Energy differences in the order of 1 kcal mol^{-1} are excellent for computations (specially involving ion pair species, in which the SMD solvent corrections are less accurate[19]). Although in this case this happens to be unfortunate, since experimentally the $AsPh_3$-catalyzed Pathway B is somewhat lower in energy than the uncatalyzed Pathway A, this contradiction (possible within the limits of calculation accuracy) does not question the quality of the DFT results and the value and correctness of the structures observed computationally along the pathway.

In conclusion, the $Rh^{I}Ar/Au^{I}Cl$ transmetalation reaction studied in this work does not involve the prototypical transition states with mixed double bridges. Instead, this exchange occurs via oxidative insertion of Au into the Rh–C bond through transition states and reaction intermediates which display short Au–Rh distances. This marked tendency for both Ar/Ar',[5] and Ar/Cl exchanges to occur via heterometallic bonded species might make to reconsider existing mechanistic proposal for other transmetalation reactions in related systems, made in the lack of experimental data and calculations. Moreover, the accelerating effect of $AsPh_3$ reveals the existence of cooperative pathways, being the ligand promoted the most feasible one. The fact that gold tricoordination eases its oxidative insertion is closely related with several examples reported recently where oxidative addition probes to be much more feasible in bent (by chelate ligands) Au^{I} species compared to their linear analogues.[20] This work, therefore, paves the way for the development of new ligand promoted processes involving gold(I) complexes, not only with chelate ligands but also via reversible ligand association equilibria.

Acknowledgements

The authors thank the financial support from the Spanish MINECO (projects CTQ2016-80913-P and CTQ2017-89217-P) and the Junta de Castilla y León (projects VA051P17 and VA062G18). The DJEI/DES/SFI/HEA Irish Centre for High-End Computing (ICHEC) is also acknowledged for the provision of computational facilities and support. M. N. P.-D. gratefully acknowledges the Spanish MECD for a FPU scholarship.

Keywords: bimetallic catalysis • oxidative addition • gold • rhodium • transmetalation mechanism • density functional theory • microkinetic modeling

[1] a) M. H. Pérez-Temprano, J. A. Casares, P. Espinet, *Chem. –Eur. J.* **2012**, *18*, 1864–1884; b) D. R. Pye, N. P. Mankad, *Chem. Sci.* **2017**, *8*, 1705–1718.

[2] a) Y. Shi, S. A. Blum, *Organometallics*, **2011**, *30*, 1776–1779; b) J. delPozo, J. A. Casares, P. Espinet, *Chem. – Eur. J.* **2016**, *22*, 4274–4284; c) R. J. Oeschger, P. Chen, *J. Am. Chem. Soc.* **2017**, *139*, 1069–1072; d) M. Oi, R. Takita, J. Kanazawa, A. Muranaka, C. Wang, M. Uchiyama, *Chem. Sci.* **2019**, *10*, 6107–6112.

[3] For detailed mechanistic study of a Pd/Au transmetalation see: M. H. Pérez-Temprano, J. A. Casares, A. R. de Lera, R. Álvarez, P. Espinet, *Angew. Chem. Int. Ed.* **2012**, *51*, 4917–4920.

[4] For the Pd/Au bimetallic application see: J. delPozo, D. Carrasco, M. H. Pérez-Temprano, M. García-Melchor, R. Álvarez, J. A. Casares, P. Espinet, *Angew. Chem. Int. Ed.* **2013**, *52,* 2189–2193.

[5] M. N. Peñas-Defrutos, C. Bartolomé, M. García-Melchor, P. Espinet, *Angew. Chem. Int. Ed.* **2019**, *58*, 3501–3505.

[6] By "oxidative insertion" we mean an oxidative addition where, being two metals involved in the redox process with formation of an M-M' bond, each metal changes only in one unit its formal oxidation number.

[7] For transmetalation reactions employing haloaryl groups see: a) A. L. Casado, P. Espinet, *Organometallics*, **1998**, *17*, 3677–3683. b) M. N. Peñas-Defrutos, C. Bartolomé, M. García-Melchor, P. Espinet, *Chem. Commun.* **2018**, *54*, 984–987. c) M. Pérez-Iglesias, O. Lozano-Lavilla, J. A. Casares, *Organometallics*, **2019**, *38*, 739–742.

[8] Note that the reversibility of transmetalations is often source of complications, such as formation of homocoupling products: J. del Pozo, G. Salas, R. Álvarez, J. A. Casares, P. Espinet, *Organometallics*, **2016**, *35*, 3604–3611; and references therein.

[9] D. Carrasco, M. García-Melchor, J. A. Casares, P. Espinet, *Chem. Commun.* **2016**, *52*, 4305–4308.

[10] Obviously only **1** and **4** are observed by ^{19}F NMR (^{1}H NMR is not informative in our case). $C_6F_3Cl_3$-1,3,5 is used as internal reference.

[11] S. Kozuch, S. Shaik, *Acc. Chem. Res.* **2011**, *44*, 101–110.

[12] S. Hoops, S. Sahle, R. Gauges, C. Lee, J. Pahle, N. Simus, M. Singhal, L. Xu, P. Mendes, U. Kummer, *Bioinformatics*, **2006**, *22*, 3067–3074.

[13] B. Cordero, V. Gómez, A. E. Platero-Prats, M. Revés, J. Echeverría, E. Cremades, F. Barragán, S. Alvarez, *Dalton Trans.* **2008**, 2832–2838.

[14] C. Bianchini, C. J. Elsevier, J. M. Ernsting, M. Peruzzini, F. Zanobini, *Inorg. Chem.* **1995**, *34*, 84–92.

[15] (a) M. C. Gimeno, A. Laguna, *Chem. Rev.* **1997**, *97*, 511–522. (b) M. A. Carvajal, J. J. Novoa, S. Alvarez, *J. Am. Chem. Soc.* **2004**, *126*, 1465–1477.

[16] $[AuCl(PPh_3)_2]$ has been thoroughly studied due to its photophysical interest: (a) M. Hoshino, H. Uekusa, S. Sonoda, T. Otsuka, Y. Kaizu, *Dalton Trans.* **2009**, 3085–3091. (b) M. Hoshino, H. Uekusa, S. Ishii, T. Otsuka, Y. Kaizu, Y. Ozawa, K. Toriumi, *Inorg. Chem.* **2010**, *49*, 7257–7265. For $[AuCl(PPh_3)_3]$ see: (c) P. G. Jones, G. M. Sheldrick, J. A. Muir, M. M. Muir, L. B. Pulgar, *J. Chem. Soc., Dalton Trans.* **1982**, 2123–2125.

[17] For [AuCl(AsPh$_3$)] see: B. Weissbart, L. J. Larson, M. M. Olmstead, C. P. Nash, D. S. Tinti, *Inorg. Chem.* **1995**, *34*, 393–395. For [AuX(AsPh$_3$)$_m$] (*m* = 2, 3 see: (b) G. A. Bowmaker, P. C. Healy, A. N. Sobolev, A. H. White, *Aust. J. Chem.* **2019**. DOI: 10.1071/CH19340. (c) P. C. Healy, A. H. White, W. T. Robinson, **2017**, CCDC number 1526150 (Private Communication).

[18] U. M. Tripathi, A. Bauer, H. Schmidbaur, *J. Chem. Soc. Dalton Trans.* **1997**, 2865–2888.

[19] A. V. Marenich; C. J. Cramer, D. G. Truhlar, *J. Phys. Chem. B* **2009**, *113*, 6378–6396.

[20] (a) M. Joost, A. Amgoune, D. Bourissou, *Angew. Chem. Int. Ed.* **2015**, *54*, 15022–15045. (b) M. Joost, A. Zeineddine, L. Estévez, S. Mallet-Ladeira, K. Miqueu, A. Amgoune, D. Bourissou, *J. Am. Chem. Soc.* **2014**, *136*, 14654−14657. (c) Y. Yang, L. Eberle, F. F. Mulks, J. F. Wunsch, M. Zimmer, F. Rominger, M. Rudolph, A. S. K. Hashmi, *J. Am. Chem. Soc.* **2019**, *141*, 17414–17420.